AGU PUBLICATIONS

Tectonics

RESEARCH ARTICLE
10.1002/2015TC003952

Key Points:
- Distribution of thermochronological data show an asymmetric exhumation starting in the NW Tatra Mountains
- Fully reset ZFT, ZHe ages indicate that the basement was heated to temperatures above 240°C.

Supporting Information:
- Figures S1–S3

Correspondence to:
A. A. Anczkiewicz,
ndstruzi@cyf-kr-edu.pl

Citation:
Anczkiewicz, A. A., M. Danišík, and J. Środoń (2015), Multiple low-temperature thermochronology constraints on exhumation of the Tatra Mountains: New implication for the complex evolution of the Western Carpathians in the Cenozoic, *Tectonics*, *34*, 2296–2317, doi:10.1002/2015TC003952.

Received 24 JUN 2015
Accepted 4 OCT 2015
Accepted article online 8 OCT 2015
Published online 18 NOV 2015

Multiple low-temperature thermochronology constraints on exhumation of the Tatra Mountains: New implication for the complex evolution of the Western Carpathians in the Cenozoic

Aneta Agnieszka Anczkiewicz[1], Martin Danišík[2], and Jan Środoń[1]

[1]Institute of Geological Sciences, Polish Academy of Sciences, Research Centre in Kraków, Kraków, Poland, [2]John de Laeter Centre for Isotope Research, Department of Applied Geology, The Institute for Geoscience Research (TIGeR), Curtin University, Perth, Western Australia, Australia

Abstract The tectonothermal evolution of the highest mountain range in the Carpathian arc—the Tatra Mountains— is investigated by zircon and apatite fission track and zircon (U-Th)/He (ZHe) dating methods in order to unravel the disputed exhumation and geodynamic processes in the Western Carpathians. Our data in combination with geological evidences reveal a complex Cenozoic history, with four major tectonothermal events: (i) a very low grade metamorphism of the crystalline basement at temperatures >240°C due to tectonic burial during the Eo-Alpine collision in the Late Cretaceous (~80 Ma); (ii) exhumation and cooling of the basement to temperatures <130°C related to postorogenic collapse during Late Cretaceous-Paleocene times; (iii) Middle Eocene-Early Miocene reheating to >150°C after burial to 5–9 km depths by the Paleogene fore-arc basin; (iv) final exhumation of the segmented basement blocks during Oligocene-Miocene (32–11 Ma) owing to lateral extrusion of the North Pannonian plate and its collision with the European foreland. The spatial pattern of thermochronological data suggests asymmetric exhumation of the Tatra Mountains, beginning in the northwest at ~30–20 Ma with low cooling rates (~1–5°C/Ma) and propagating toward the major fault bounding the range in the south, where the youngest cooling ages (16–9 Ma) and fastest cooling rates (~10–20°C/Ma) are found. Our data prove that the Tatra Mountains shared Cenozoic evolution of other crystalline core mountains in the Western Carpathians. However, the Miocene ZHe ages suggest that the Tatra Mountains were buried to the greatest depths in the Paleogene-Early Miocene and experienced the greatest amount of Miocene exhumation.

1. Introduction

The Western Carpathians represent the northernmost branch of the Alpine orogenic belt in Europe (Figure 1). They have experienced a complex Alpine tectonothermal evolution, comprising Jurassic rifting and basin formation, Cretaceous collisional tectonics, extensional collapse, lateral tectonic extrusion of a fragment of the Adriatic plate (so called ALCAPA or North Pannonian block), and intricate interaction of that fragment with the European foreland in the Tertiary period, leading to the formation of an accretionary wedge with thin-skinned thrusts in the foreland and coeval back-arc extension forming the Pannonian basin system in the hinterland [e.g., *Behrmann et al.*, 2000; *Csontos*, 1995; *Frisch et al.*, 2000; *Plašienka et al.*, 1997; *Ratschbacher et al.*, 1991a, 1991b; *Royden et al.*, 1982, 1983; *Sperner et al.*, 2002; *Tari et al.*, 1992, 1999; *Wortel and Spakman*, 2000]. Although the principal geodynamic processes of the Western Carpathian orogen are, in general, qualitatively well described by conceptual models [e.g., *Kováč et al.*, 1994, 2007; *Plašienka et al.*, 1997; *Ratschbacher et al.*, 1991a; *Sperner et al.*, 2002], a number of fundamental questions regarding the Alpine collisional and postcollisional evolution (e.g., timing and grade of metamorphism, timing, rate and nature of burial, and exhumation processes) remain controversial. For instance, two contradictory models of postcollisional exhumation evolution of Western Carpathian crystalline core complexes have been put forward. A traditional view is that the Variscan crystalline basement complexes experienced a simple, steady state cooling [*Kováč et al.*, 1994]. In contrast, a complex thermal history has been suggested with at least one phase of reheating related to sedimentary burial in the Paleogene or Neogene, and/or Miocene mantle upwelling associated with increased heat flow [e.g., *Danišík et al.*, 2004, 2008a, 2008b, 2010, 2011, 2015].

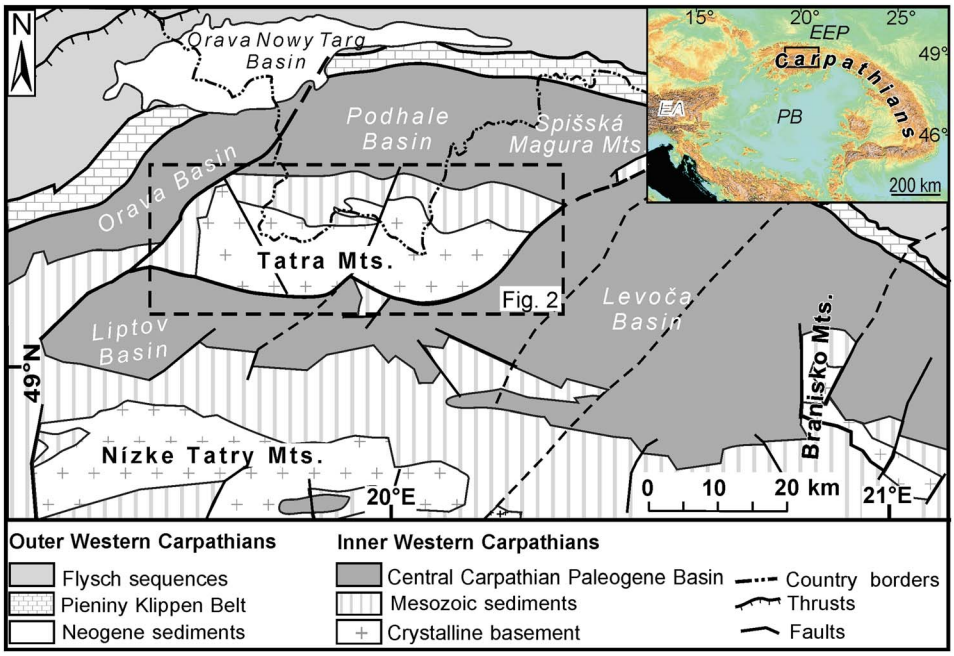

Figure 1. Simplified tectonic map of the Western Carpathians after *Żytko et al.* [1989]. Black rectangle: study area. Inset: the location of map.

In this study we target the Tatra Mountains—a ~57 km long and ~19 km wide, prominent mountain range in the Western Carpathians, which, with Gerlach Peak (2655 m above sea level (asl)), represents the topographically highest mountain range in the entire Carpathian Arc. While the well-known Late Cretaceous (Eo-Alpine) collision in the Western Carpathians has been documented in the Tatra Mountains by numerous independent pieces of evidence, including K-Ar geochronology, paleomagnetic, and stratigraphic data [*Lefeld*, 1997; *Maluski et al*., 1993; *Środoń et al*., 2006; *Wolska et al*., 2002], the subsequent posttectonic exhumation history has been a matter of discussion for more than 40 years. This is due to the very limited Cenozoic geological record in the area, the low number of high-quality low-temperature thermochronological data that would allow quantitative reconstruction of burial/exhumation history, and the lack of compelling seismic data that would allow to understand the deep structure of the mountain range.

From a historical perspective it is noteworthy that the Tatra Mountains was one of the first areas investigated by the fission track dating method. Already in 1970s of the last century, *Burchart* [1972] and *Kráľ* [1977] reported apatite fission track ages of 37–10 Ma from the Tatra Mountains and interpreted them as recording a Late Eocene to Miocene exhumation of the basement rocks. It has to be acknowledged that these pioneering data were measured by the antiquated population dating method and without the use of high-power microscopy and computer-automated stages for accurate (re)locating and counting of fission tracks. Thus, the difference between some of their ages and modern data (collected by using modern technologies and refined analytical procedures) has led to misleading interpretations in the past, but should in no way be seen as a reason for criticism of these heroic achievements. A great deal of thermochronological data, including zircon and apatite fission track and (U-Th)/He dating of zircon and apatite, has been reported by several research teams in the last ~13 years [*Anczkiewicz et al*., 2005; *Baumgart-Kotarba and Kráľ*, 2002; *Králiková et al*., 2014; *Struzik et al*., 2002; *Śmigielski et al*., 2010, 2011, 2012]. A compilation of reported ages shows a wide scatter spanning from 45 Ma to 2 Ma, whereby individual data sets have been interpreted in different ways, including differential exhumation of segmented basement blocks, varying burial depths in the Early Tertiary, Quaternary erosion related to topographic growth or imprecision of the applied analytical techniques [*Anczkiewicz et al*., 2005; *Baumgart-Kotarba and Kráľ*, 2002; *Struzik et al*., 2002; *Śmigielski et al*., 2010, 2011, 2012]. Unfortunately, most of the data were published as conference abstracts, and none of these studies provide critical information such as sample location, analytical procedures, or analytical results. Consequently, it is not possible to evaluate the quality of the reported data, investigate spatial distributions and trends, and ultimately reconstruct the tectonothermal history.

In this study, we seek to clarify the diverse geodynamic models proposed for the Tatra Mountains, by applying zircon and apatite fission track (ZFT and AFT, respectively) and zircon (U–Th)/He (ZHe) dating methods, which cover the temperature range of 240–60°C [e.g., *Brandon et al*., 1998; *Hurford*, 1986; *Reiners et al*., 2004]. We also report the first comprehensive thermochronological data set based on a large number of samples ($n = 35$), systematically collected across the Tatra Mountains which allows us to examine the disparity in previously published ages. Our new data, in combination with available geological constraints, allow us to identify and quantify the timing and rates of cooling/heating episodes and reconstruct the metamorphic, exhumation and burial history of the Tatra Mountains throughout the Cenozoic era, which have implications for elucidating the geodynamic evolution of the Western Carpathians and thus the European Alpine chain in general.

2. Geological Setting

The Western Carpathians form the northernmost and the westernmost segment of the Carpathian orogenic belt, which represents an eastern continuation of the Eastern Alps (Figure 1). They are traditionally subdivided into two main tectonic domains—the Outer and the Inner Western Carpathians [*Birkenmajer*, 1986; *Książkiewicz*, 1977]. The Outer Western Carpathians (OWC) form a nappe stack of lower Cretaceous to lower Miocene flysch sequences, which developed by northward thrusting of several basins at the northern margin of the Tethys ocean during the collision of the North Pannonian (ALCAPA) block with the European plate in the Early-Middle Miocene [e.g., *Csontos et al*., 1992; *Nemčok et al*., 1989; *Rögl*, 1996; *Sperner et al*., 2002]. The OWC are separated from the Inner Western Carpathians by the Pieniny Klippen Belt—a narrow, E-W trending suture zone comprising strongly deformed carbonates of Jurassic to Cretaceous age, interpreted as a plate boundary between the European plate to the north and the North Pannonian block to the south [*Biely*, 1989; *Birkenmajer*, 1986; *Nemčok and Nemčok*, 1994; *Nemčok et al*., 1989; *Ratschbacher et al*., 1993; *Rögl*, 1996; *Sperner et al*., 2002]. The Inner Western Carpathians (IWC) comprise Variscan crystalline basement core complexes with autochthonous Upper Paleozoic-Mesozoic sedimentary cover overlain by Mesozoic nappes, posttectonic Paleogene flysch sediments of the so-called Central Carpathian Paleogene Basin (CCPB), Neogene sediments of the Pannonian Basin, and Neogene volcanic rocks [e.g., *Lexa et al*., 2000].

The Tatra Mountains mark the northernmost basement core complex of the IWC. The complex consists (from the bottom to the top) of the following: (i) the crystalline basement core that formed during the Variscan orogeny in the Carboniferous and constitutes a major portion of the mountain range [e.g., *Janák*, 1994; *Janák et al*., 1996, 1999; *Nemčok et al*., 1993; *Nemčok and Nemčok*, 1994; *Putiš*, 1992]. The basement core is composed of magmatic rocks (granites, granodiorites, and tonalites) dated as 350–290 Ma (U-Pb and Rb-Sr data) [*Burchart*, 1968; *Burda et al*., 2013; *Gawęda*, 1995; *Gawęda et al*., 2014; *Poller et al*., 1999, 2000; *Poller and Todt*, 2000], and by medium- to high-grade metamorphic rocks (gneisses, migmatites, mica-schists, and amphibolites) with metamorphic ages of 357–322 Ma (Ar/Ar data) [*Dallmeyer et al*., 1993, 1996; *Kohút and Sherlock*, 2003; *Maluski et al*., 1993; *Moussallam et al*., 2012], exposed in the western part of the range [*Janák*, 1994; *Janák et al*., 1996, 1999; *Nemčok et al*., 1993; *Nemčok and Nemčok*, 1994; *Putiš*, 1992]; (ii) autochtonous Upper Paleozoic-Mesozoic sedimentary cover, contouring the crystalline core from the north [*Plašienka et al*., 1997; *Plašienka*, 2003]; and (iii) two allochthonous nappes (the so-called Krížna Nappe (Fatricum) and Choč Nappe (Hronicum)) [*Plašienka et al*., 1997] that are composed of analogous Mesozoic rocks preserved mostly along the northern margin of the range (Figure 2a).

The Mesozoic nappes were thrust onto the Variscan crystalline basement and its sedimentary cover during the Eo-Alpine shortening in the Late Cretaceous (~93–89 Ma; Turonian) [e.g., *Andrusov*, 1965; *Andrusov et al*., 1973; *Plašienka*, 2003]. The thickness of the individual Mesozoic nappes was probably quite variable but never exceeded 2 km as estimated from the lithological columns [*Nemčok et al*., 1993]. The degree of Alpine metamorphic overprint on the crystalline basement is still a matter of discussion. While some authors argued for no or only a very weak metamorphic condition (i.e., anchizonal to lower greenschist facies) restricted to shear zones [e.g., *Krist et al*., 1992; *Plašienka et al*., 1997; *Plašienka*, 2003], others argued for a distinct Alpine overprint of the crystalline basement and cover units to low-grade metamorphic conditions [e.g., *Jurewicz and Kozłowski*, 2003; *Kotarba*, 2003; *Wolska et al*., 2002]. The arguments supporting the Alpine metamorphic overprint include PT estimates of ~212–254°C/~145–170 MPa based on fluid inclusions

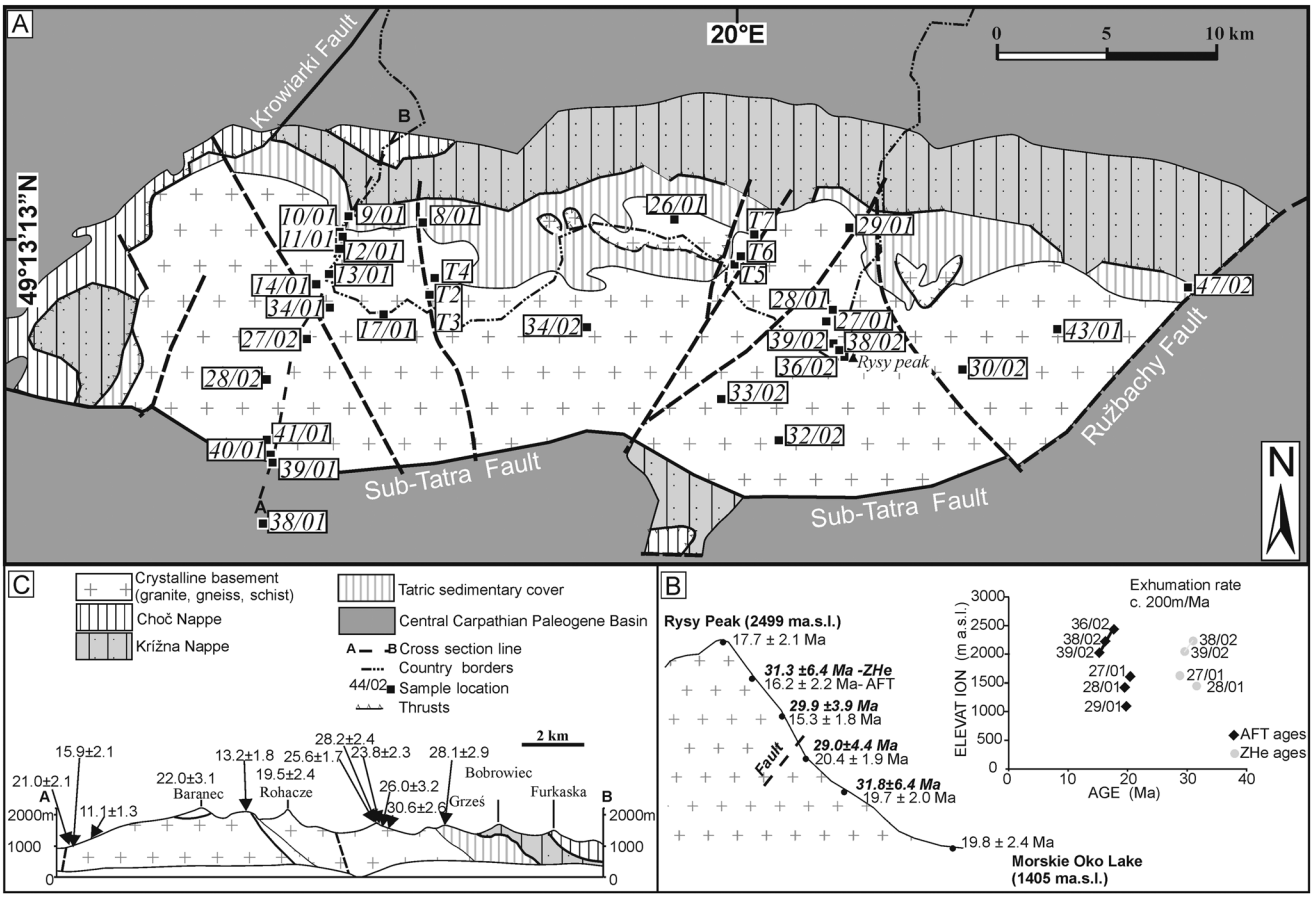

Figure 2. (a) Sample locations from the Tatra Mountains depicted on a simplified geological map after *Żytko et al.* [1989]. (b) AFT and ZHe age-elevation diagram for samples from the Rysy Peak with calculated exhumation rate. (c) Cross section along the Western Tatra Mountains.

thermobarometry data [*Jurewicz and Kozłowski*, 2003], Cretaceous reset of Ar/Ar and K/Ar systems in some micas from Triassic bentonite and "pietra verde" type tuffite (suggesting temperatures of ≥300–350°C) [*Kotarba*, 2003; *Maluski et al.*, 1993; *Koszowska et al.*, 1998, 2001; *Wolska et al.*, 2002], and remagnetization of the carbonates in the Mesozoic nappe indicative of temperatures ≥150°C [*Grabowski*, 1997]. Finally, conodont alteration index values (~1.5–2) and vitrinite reflectance data (0.9–1.8%) suggest maximum burial temperatures of ~50–140°C and 105–150°C, respectively [*Grabowski et al.*, 1999; *Marynowski et al.*, 2001, 2006; *Poprawa et al.*, 2002].

The postthrusting evolution is less clear as there are no post-Late Cretaceous sediments preserved directly on the mountain range but only in the surrounding basins. Nappe stacking was likely followed by postorogenic collapse [e.g., *Plašienka et al.*, 1997; *Ratschbacher et al.*, 1991a, 1991b; *Sperner et al.*, 2002] associated with erosion of Mesozoic nappes and exhumation of the Variscan crystalline core and its cover sequences, lasting until the Paleocene-Early Eocene. This is evidenced by components of Triassic and Liassic rocks found in the basal conglomerates of the next (Eocene) sedimentation cycle [*Lefeld*, 1985, 1997; *Roniewicz*, 1969] and by late Cretaceous-earliest Paleocene $^{40}Ar/^{39}Ar$ ages on mica (75 ± 1 to 63 ± 1 Ma) [*Maluski et al.*, 1993] and ZFT ages (76.8 ± 11 to 63.9 ± 11 Ma) [*Králiková et al.*, 2014] pointing to a cooling of the basement at that time. It has been argued that even some parts of the crystalline basement in the western part of the Tatra Mountains could have been exhumed to the surface as the Eocene transgressive sedimentary sequence (see below) was deposited directly on the exposed basement rocks (e.g., at locality Košariská) [*Andrusov*, 1959; *Nemčok et al.*, 1994].

In the Middle Eocene, a fore-arc basin (Central Carpathian Paleogene Basin, CCPB) developed along the northern margin of the ALCAPA microplate, close to the accretionary wedge of the OWC [*Kázmér et al.*, 2003].

The new sedimentation cycle began in the Lutetian (49–42 Ma) with a marine transgression and deposition of the Nummulitic Eocene and continued with carbonate platform development and flysch deposition lasting until the earliest Miocene [*Bieda*, 1959, 1963; *Garecka*, 2005; *Gedl*, 1999; *Gross et al*., 1984, 1993; *Olszewska and Wieczorek*, 1998; *Soták et al*., 2001; *Soták*, 2010; *Starek et al*., 2012; *Tokarski et al*., 2012]. The CCPB sediments envelope the Tatra Mountains in series of basins, including Podhale Basin in the north, Orava Basin in the west, Spiš Basin in the east, and Liptov Basin in the south. However, whether or not the Paleogene sedimentation cycle influenced the cooling evolution of the basement is still unclear, as is the amount of CCPB strata removed during Neogene erosion. Some authors [e.g., *Kohút and Sherlock*, 2002] assumed no Paleogene cover on the Tatra Mountains. In contrast, based on paleocurrent measurements in Eocene and Oligocene sediments, *Marschalko* [1968] suggested that no positive morphological feature existed at the location of the present-day Tatra Mountains, suggesting a complete burial of the range. A Late Eocene-Oligocene AFT age of ~37–24 Ma reported by *Burchart* [1972] and *Kráľ* [1977] has been interpreted as marking the exhumation of the massif to surface at that time. In contrast, Miocene AFT ages [*Anczkiewicz et al*., 2005; *Baumgart-Kotarba and Kráľ*, 2002; *Burchart*, 1972; *Kráľ*, 1977; *Králiková et al*., 2014; *Struzik et al*., 2002; *Śmigielski et al*., 2010, 2011, 2012], the significant thickness of Paleogene sediments in the surrounding basins [*Soták et al*., 2001], fluid inclusion data [*Hurai et al*., 2000], and analogy with other core mountains in the IWC [cf. *Danišík et al*., 2004, 2008a, 2008b, 2010, 2012] may suggest a significant burial in the Paleogene followed by an exhumation in the Neogene.

Inversion and disintegration of the CCPB basin started in the Late Oligocene-Early Miocene times in the course of the lateral extrusion and NEE-NE movement of the ALCAPA microplate [*Ratschbacher et al*., 1991a, 1991b; *Nemčok*, 1993; *Sperner et al*., 2002]. This process was accompanied by extension in the Pannonian region. Subsequently, another sedimentation cycle, represented by transgression of the Pannonian Sea, commenced in the IWC, during the Early Miocene. None of these sediments are preserved directly in the study area; however, $>$1 km of Middle Miocene-Pliocene sediments are preserved in the small Orava-Nowy Targ Basin located ~10 km north of the Tatra Mountains (Figure 1) [*Gross et al*., 1993; *Tokarski et al*., 2012; *Wagner*, 2011; *Watycha*, 1976].

Quaternary sediments are represented by alluvial fans and glacigenic sediments reaching a few hundred meters in thickness and found in the southern foothills of the western Tatra Mountains [*Birkenmajer*, 2009; *Nemčok*, 1993].

At present, the Tatra Mountains forms a prominent horst structure that must have existed in the Pleistocene as evidenced by glacigenic sediments. The youngest sediments in the area of the Tatra Mountains are related to Pleistocene glaciation and to Holocene erosion and accumulation processes. Pleistocene sediments are dominated by glacial moraine and fluvial deposits while the Holocene rocks are represented by unconsolidated sediments, mainly sands, silt, and gravels as well as alluvial soils, peat, and peat silts [*Bac-Moszaszwili and Jurewicz*, 2010; *Jurewicz*, 2005]. Structural data and preservation of the Mesozoic cover units along the northern margin of the range suggest that the Tatra Mountains was asymmetrically uplifted and tilted by 40° toward the north along the Sub-Tatra fault—a major fault bounding the range from the south [*Bac-Moszaszwili et al*., 1984; *Jurewicz*, 2000; *Piotrowski*, 1978; *Sokołowski*, 1959; *Uhlig*, 1899]. The Tatra Mountains massif is cut by NE-SW trending tectonic zones, which developed during the Alpine orogenesis in the Late Cretaceous [*Sperner et al*., 2002], and some of them were reactivated in the Neogene and Quaternary [*Vojtko et al*., 2010].

3. Samples and Methods

3.1. Sampling Strategy

To fully examine the regional pattern of exhumation, we collected 32 samples from the crystalline basement and three samples from Triassic sediments of the autochthonous sedimentary cover, all regularly distributed across the Tatra Mountains (Figure 2a and Table 1). In addition, one sample of Lower Oligocene (Rupelian) sandstone from the CCPB was collected from the Liptov Basin south of the Sub-Tatra fault, in order to give an indication of the magnitude of postdepositional reheating and to investigate differential block movements along the major fault. To better constrain exhumation rates, one steep elevation profile of six samples was collected every ~200 m over 1000 m elevation along the trail to the top of the Rysy peak (2499 m asl) (Figure 2b).

Table 1. Zircon and Apatite Fission Track Results[a]

Sample No	Rocks type	Location GPS	Elevation (m asl)	No. of Crystals	U (ppm)	Dosimeter		Spontaneous		Induced		$P(\chi^2)$ (%)	Central Age (Ma) ± 1σ	Average Length (μm) (± SE)	SD	Amount of Measured Tracks	Dpar
						ρ_d	Nd	ρ_s	Ns	ρ_i	Ni						
Zircon Fission Track Dating																	
41/01	Gneiss	N 49°09.003′ E 19°44.402′	1248	16	21629.2	0.7039	4942	397.5469	551	411.9769	571	4.48	55.2 ± 4.3				
Apatite Fission Track Dating																	
8/01	Sandstone	N 49°13.992′ E 19°49.623′	1290	14	10.71	1.029	3010	0.1306	77	0.9361	552	69.2	24.9 ± 3.2	nd			1.5
9/01	Sandstone	N 49°14.529′ E 19°46.383′	1522	19	19.36	1.024	3010	0.2304	328	1.6876	2402	0	28.1 ± 2.9	nd			1.5
10/01	Gneiss	N 49°13.971′ E 19°46.047′	1629	20	18.58	1.111	5137	0.2695	169	1.6775	1052	99.98	30.6 ± 2.6	12.40 ± 0.60	2.3	15	1.5
11/01	Gneiss	N 49°13.955′ E 19°46.060′	1629	20	8.01	0.9809	4816	0.0979	79	0.6347	512	100	26.0 ± 3.2	11.90 ± 0.68	3.0	23	1.5
12/01	Gneiss	N 49°13.586′ E 19°46.020′	1646	20	16.37	1.066	3232	0.1805	129	1.3911	994	100	23.8 ± 2.3	12.50 ± 0.52	2.5	24	1.6
13/01	Gneiss	N 49°12.986′ E 19°45.500′	1879	20	20.93	1.096	5137	0.2851	161	1.9036	1075	100	28.2 ± 2.4	11.20 ± 0.61	1.8	9	1.6
14/01	Granite	N 49°12.786′ E 19°45.095′	1879	19	50.45	1.11	3232	0.6025	298	4.4925	2222	100	25.6 ± 1.7	12.90 ± 0.35	2.4	57	1.5
17/01	Gneiss	N 49°11.879′ E 19°48.037′	2176	19	25.71	1.095	3232	0.2662	158	2.2948	1362	100	21.8 ± 1.9	11.10 ± 0.50	2.79	31	1.6
26/01	Granite	N 49°14.480′ E 19°58.567′	1652	20	35.62	1.065	5137	0.3412	233	3.1061	2121	100	20.1 ± 1.4	13.70 ± 0.49	2.1	23	1.5
27/01	Granite	N 49°11.394′ E 20°04.257′	1610	20	17.91	1.075	5137	0.1723	135	1.5555	1219	100	20.4 ± 1.9	12.20 ± 0.25	1.8	59	1.5
28/01	Granite	N 49°11.625′ E 20°04.378′	1436	20	17.89	1.14	5492	0.1655	110	1.6416	1091	100	19.7 ± 2.0	11.80 ± 0.56	2.2	17	1.5
29/01	Granite	N 49°14.072′ E 20°05.243′	1080	20	10.13	1.054	5137	0.0935	75	0.8554	686	100	19.8 ± 2.4	12.98 ± 0.49	2.23	20	1.5
34/01	Granite	N 49°12.040′ E 19°45.515′	2078	20	13	1.135	5492	0.1226	75	1.2259	750	100	19.5 ± 2.4	12.10 ± 0.56	2.5	24	1.4
38/01	Sandstone	N 49°07.080′ E 19°44.242′	760	19	12.36	1.117	5137	0.1263	57	1.09	492	100	22.2 ± 3.1	nd			1.8
39/01	Schist	N 49°08.289′ E 19°44.577′	916	20	18.73	1.14	5492	0.1859	120	1.7323	1118	100	21.0 ± 2.1	12.40 ± 0.48	2.5	30	1.5
40/01	Gneiss	N 49°08.471′ E 19°44.560′	940	18	15.02	0.999	4816	0.1176	63	1.267	679	100	15.9 ± 2.1	13.76 ± 0.40	1.41	12	1.6
41/01	Gneiss	N 49°09.003′ E 19°44.402′	1248	20	24.65	0.9962	4816	0.1294	83	1.9999	1283	100	11.1 ± 1.3	12.80 ± 0.53	2.1	28	1.5
43/01	Granite	N 49°11.384′ E 20°11.963′	2003	20	19.69	1.0	4816	0.087	53	1.6111	981	100	9.3 ± 1.3	nd			1.4
T 2	Granite	N 49°12.253′ E 19°50.113′	1880	20	62.89	1.205	5912	0.6406	352	6.3919	3512	12.55	20.8 ± 1.3	13.65 ± 0.30	1.79	36	1.4
T 3	Schist	N 49°12. 253′ E 19°50.113′	1880	20	51.55	1.206	5912	0.4561	375	5.2963	4355	0.69	18.4 ± 1.3	13.96 ± 0.24	1.51	40	1.6
T 4	Granite	N 49°12.871′ E 19°50.271′	1867	20	16.51	1.073	3232	0.1544	133	1.2339	1063	99.35	23.0 ± 2.2	13.55 ± 0.64	1.93	9	1.5
T 5	Granite	N 49°13.301′ E 20°01.149′	1820	20	17.58	1.215	5912	0.1021	82	1.9072	1532	57	11.2 ± 1.3	13.49 ± 0.35	2.06	34	1.4
T 6	Granite	N 49°13.468′ E 20°01.369′	1800	20	15.6	1.214	5912	0.0808	50	1.506	932	37.46	11.2 ± 1.7	12.74 ± 0.50	2.01	16	1.4
T 7	Granite	N 49°13.786′ E 20°01.562′	1670	20	13.71	1.231	5912	0.0739	52	1.4003	985	97.01	11.2 ± 1.6	13.12 ± 0.40	1.43	13	1.4
27/02	Schist	N 49°11.394′ E 19°45.174′	2021	20	21.03	1.142	5492	0.1328	62	1.9689	919	100	13.2 ± 1.8	12.00 ± 0.57	2.9	32	1.6
28/02	Granite	N 49°10.410′	2185	20	13.66	1.137	5492	0.1398	58	1.2389	514	100	22.0 ± 3.1	13.17 ± 0.29	1.63	30	1.6

AGU Tectonics

10.1002/2015TC003952

Table 1. (continued)

Sample No	Rocks type	Location GPS	Elevation (m asl)	No. of Crystals	U (ppm)	Dosimeter		Spontaneous		Induced		$P(\chi^2)$ (%)	Central Age (Ma) ± 1σ	Average Length (μm) (± SE)	SD	Amount of Measured Tracks	Dpar
						ρ_d	Nd	ρ_s	Ns	ρ_i	Ni						
		E 19°44.442′															
30/02	Granite	N 49°10.518′ E 20°08.729′	2428	20	15.46	1.137	5492	0.0956	63	1.4237	938	100	13.1 ± 1.7	12.97 ± 0.46	1.96	18	1.5
32/02	Granite	N 49°08.814′ E 20°02.415′	1970	20	14.98	1.134	5492	0.0789	37	1.3485	632	100	11.4 ± 1.9	13.01 ± 0.34	1.38	16	1.5
33/02	Granite	N 49°09.869′ E 20°00.152′	2495	20	15.33	1.141	5492	0.0789	36	1.4051	641	100	11.0 ± 1.9	12.58 ± 0.22	0.94	17	1.4
34/02	Granite	N 49°11.187′ E 19°54.999′	1100	20	11.43	1.139	5492	0.0798	44	0.9796	540	100	15.9 ± 2.5	11.39 ± 0.36	2.35	43	1.5
36/02	Granite	N 49°10.772′ E 20°05.287′	2499	20	21.04	1.085	5137	0.1771	82	1.8621	862	100	17.7 ± 2.1	13.70 ± 0.60	2.1	25	1.5
38/02	Granite	N 49°10.835′ E 20°05.044′	2224	20	13.41	1.138	5492	0.1002	59	1.2128	714	100	16.2 ± 2.2	14.10 ± 0.25	2.1	20	1.5
39/02	Granite	N 49°10.874′ E 20°04.853′	2035	20	20.31	1.049	5137	0.1467	83	1.7324	980	100	15.3 ± 1.8	12.50 ± 0.38	2.5	52	1.5
47/02	Mudstone	N 49°12.994′ E 20°18.231′	800	20	21.79	0.989	4816	0.1911	89	1.7218	802	100	18.9 ± 2.1	13.60 ± 0.76	1.9	12	1.5

[a] ρ_s: density of spontaneous tracks ($\times 10^6$ tracks/cm^2); N_s: number of spontaneous tracks; ρ_i: density of induced tracks in external detector ($\times 10^6$ tracks/cm^2); N_i: number of induced tracks; ρ_d: density of induced tracks in external mica detector covering dosimeter CN2 (zircon) and CN5 (apatite) glasses ($\times 10^6$ tracks/cm^2); N_d: number of tracks counted on dosimeter; $P(\chi^2)$ is the probability obtaining chi-square value (χ^2) for n degrees of freedom (where n = number of crystals − 1) [*Galbraith*, 1981; *Green*, 1981]; Dpar: average etch pit diameter of fission tracks; AFT ages are central ages ±1σ uncertainty calculated after *Galbraith and Laslett* [1993]. The external detector method and the ζ calibration approach was used to determine the fission tracks age [*Gleadow*, 1981; *Hurford and Green*, 1983], with the ζ values of 344 ± 5 for CN5 and 165.06 ± 1.79 for CN2 glass dosimeters (operator: A.A. Anczkiewicz).

3.2. Analytical Techniques

3.2.1. Apatite and Zircon Fission Track

ZFT and AFT dating by the external detector method [*Gleadow et al.*, 1983] was carried out at the Institute of Geological Sciences, Polish Academy of Sciences in Krakow (Poland). Zircon and apatite crystals were mounted in PFA teflon^{TM} sheets and epoxy resin, respectively, polished and etched in NaOH–KOH eutectic melt at 225°C for 8–14 h (zircon) and 5 M HNO_3 at 20°C for 20 s (apatite) to reveal spontaneous fission tracks [*Donelick et al.*, 1999; *Zaun and Wagner*, 1985]. Samples together with age standards (Fish Canyon, Durango, and Mount Dromedary zircon and apatite) and CN2 and CN5 glass dosimeters were irradiated at the TRIGA reactor (Oregon State University, USA). After the irradiation, muscovite detectors were etched for 45 min in 40% HF to reveal induced fission tracks. Tracks were counted and track lengths were measured at 1250X magnification under an oil (zircon) and dry objective (apatite) using a NIKON Eclipse E-600 microscope, equipped with motorized stage, digitizing tablet, and drawing tube controlled by FTStage 4.04 software [*Dumitru*, 1993]. Fission track ages were calculated using TrackKey 4.2 g [*Dunkl*, 2002]. The track annealing kinetics in apatite were assessed by measuring etch pit diameter (Dpar) [*Burtner et al.*, 1994] and also by measuring chlorine content in apatites by electron microprobe CAMECA SX-100 in the Institute of Mineralogy and Geochemistry, University of Warsaw (Poland), applying 20 nA beam current and 15 kV accelerating voltage.

3.2.2. Zircon (U-Th)/He

ZHe analysis was carried out in Waikato Thermochronology Laboratory (New Zealand) following the analytical procedures described in *Danišík et al.* [2012]. Zircon crystals were hand picked following strict selection criteria [*Farley*, 2002; *Reiners*, 2005], then photographed and measured, then loaded in Nb tubes, degassed at ~1250°C under ultrahigh vacuum using a diode laser and analyzed for ^{4}He by isotope dilution on a

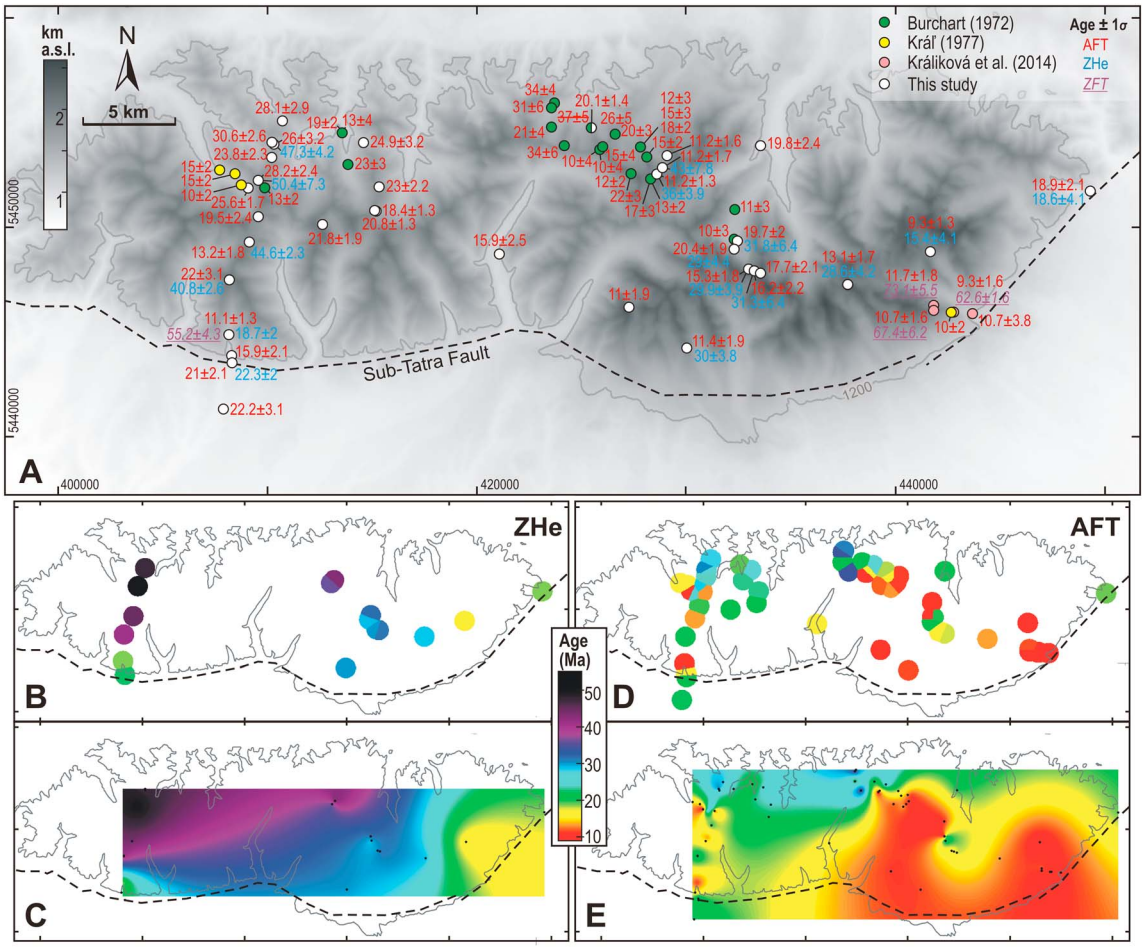

Figure 3. (a) Database of all published low-temperature thermochronology data (ages in Ma) from the Tatra Mountains displayed on a digital elevation model. The strikethrough ages from older studies are considered erroneous. Color-coded presentation in the form of (b, d) circles and (c, e) interpolation clearly shows a southward/(south easternward) younging trend. We acknowledge that interpolated areas without any data points should be interpreted with caution.

Pfeiffer Prisma QMS-200 mass spectrometer. Degassed zircon was dissolved following the procedure of *Evans et al.* [2005] and analyzed by isotope dilution for U, Th. and by external calibration for Sm on a Perkin Elmer SCIEX ELAN DRC II ICP-MS. The total analytical uncertainty (TAU) was calculated as a square root of the sum of squares of uncertainty on He and weighted uncertainties on U, Th, Sm, and He measurements, and is typically $<3\%$ (1σ). The raw ZHe ages were corrected for alpha ejection (Ft correction) after *Farley et al.* [1996], whereby a homogenous distribution of U, Th, and Sm was assumed for the crystals. Replicate analyses of Fish Canyon Tuff zircon ($n = 12$) measured over the period of this study as internal standards yielded mean ZHe age of 28.5 ± 0.9 Ma, which is in excellent agreement with the reference age of 28.3 ± 1.3 Ma [*Reiners*, 2005].

The low-temperature thermal history based on thermochronological data was modeled by the HeFTy modeling program [*Ketcham*, 2005] operated with the multikinetic fission track annealing model of *Ketcham et al.* [2007] using Dpar as kinetic parameter. For the helium diffusion kinetics in zircon we adopted the model of *Guenthner et al.* [2013] as it should better account for the radiation damage than the traditionally used diffusion model of *Reiners et al.* [2004].

4. New Results and Comparison With Existing Data

4.1. ZFT and ZHe Data

Reconnaissance ZFT dating of a basement sample (41/01) from the SW margin of the Tatra Mountains revealed an age of 55.2 ± 4.3 Ma (Table 1 and Figure 3a), which is significantly older than the corresponding

Table 2. Zircon (U-Th)/He Results[a]

Zircon (U-Th-Sm)/He Data From Tatra Mountains

Sample Code	Nc	232Th (ng)	± (%)	238U (ng)	± (%)	147Sm (ng)	± (%)	He (ncc)	± (%)	TAU (%)	eU	Th/U	Raw Age (Ma)	±1σ (Ma)	Ft	± (%)	Cor. Age (Ma)	±1σ (Ma)
11/01-1	1	0.110	1.7	0.240	2.2	0.008	50.9	0.789	1.2	2.3	377.9	0.45	24.4	0.6	0.60	5	40.9	2.2
11/01-2	1	0.162	1.6	0.343	2.1	0.002	23.4	1.542	1.2	2.2	719.9	0.47	33.2	0.7	0.64	5	51.6	2.8
11/01-3	1	0.180	1.6	0.257	2.2	0.002	25.1	1.077	1.2	2.2	385.8	0.69	29.5	0.7	0.62	5	47.5	2.5
11/01-4	1	0.056	1.9	0.358	2.1	0.003	24.9	1.391	1.2	2.3	561.1	0.15	30.8	0.7	0.61	5	50.5	2.7
11/01-5	1	0.197	1.6	0.295	2.1	0.000	16.1	1.235	1.2	2.2	329.0	0.66	29.7	0.7	0.60	5	49.3	2.6
Weighted average ± SD																	47.3	4.2
13/01-1	1	0.168	1.6	0.830	2.2	0.000	20.3	4.406	1.2	2.4	535.9	0.20	41.5	1.0	0.79	5	52.5	2.8
13/01-2	1	0.194	1.6	1.201	2.0	0.005	27.3	6.319	1.2	2.3	681.0	0.16	41.5	1.0	0.81	5	51.2	2.7
13/01-3	1	0.314	1.6	1.935	2.2	0.008	43.9	10.042	1.2	2.4	774.5	0.16	41.0	1.0	0.80	5	51.0	2.7
13/01-4	1	0.139	1.6	0.943	2.1	0.009	41.5	6.384	1.2	2.3	688.4	0.15	53.5	1.2	0.85	5	62.8	3.4
13/01-5	1	0.197	1.6	1.156	2.1	0.004	25.8	5.036	1.2	2.3	617.2	0.17	34.3	0.8	0.81	5	42.4	2.3
Weighted average ± SD																	50.4	7.3
27/01-1	1	0.157	1.6	1.873	2.0	0.005	36.8	5.120	1.2	2.3	842.0	0.08	22.0	0.5	0.77	5	28.6	1.5
27/01-2	1	0.177	1.6	2.399	2.1	0.005	32.6	8.532	1.2	2.4	720.6	0.07	28.7	0.7	0.78	5	36.7	2.0
27/01-3	1	0.170	1.6	0.621	2.1	0.003	28.9	1.448	1.2	2.3	355.7	0.27	18.0	0.4	0.73	5	24.5	1.3
27/01-4	1	0.113	1.7	2.117	2.0	0.002	19.1	5.827	1.2	2.3	914.9	0.05	22.3	0.5	0.76	5	29.5	1.6
27/01-5	1	0.317	1.6	1.525	2.1	0.007	25.7	4.621	1.2	2.3	688.3	0.21	23.7	0.5	0.77	5	30.7	1.6
Weighted average ± SD																	29.0	4.4
28/01-1	1	0.154	1.6	1.084	2.1	0.005	37.0	2.822	1.2	2.4	1150.3	0.14	20.7	0.5	0.58	10	35.7	3.6
28/01-2	1	0.130	1.6	0.860	2.0	0.004	36.4	1.994	1.2	2.3	543.4	0.15	18.4	0.4	0.56	10	32.6	3.3
28/01-3	1	0.221	1.6	0.684	2.1	0.001	44.2	2.250	1.2	2.3	965.6	0.32	25.1	0.6	0.64	5	39.3	2.1
28/01-4	1	0.082	2.0	0.728	2.7	0.004	58.0	1.119	1.2	2.9	955.4	0.11	12.3	0.4	0.53	10	23.3	2.4
28/01-5	1	0.134	1.6	0.733	2.1	0.003	47.0	1.482	1.2	2.3	1498.6	0.18	15.9	0.4	0.58	10	27.5	2.8
Weighted average ± SD																	31.8	6.4
39/01-1	1	0.371	1.6	1.418	2.1	0.009	37.5	2.916	1.2	2.3	1674.2	0.26	15.9	0.4	0.71	5	22.4	1.2
39/01-2	1	0.382	1.6	0.888	2.2	0.005	43.5	2.004	1.2	2.3	920.3	0.43	16.8	0.4	0.73	5	23.0	1.2
39/01-3	1	0.175	1.6	0.857	2.1	0.003	46.3	1.812	1.2	2.3	1002.8	0.20	16.6	0.4	0.73	5	22.9	1.2
39/01-4	1	0.385	1.6	1.065	2.0	0.004	28.7	2.682	1.2	2.2	567.3	0.36	19.1	0.4	0.76	5	25.1	1.4
39/01-5	1	0.102	1.7	0.395	2.1	0.009	36.2	0.675	1.2	2.3	262.4	0.26	13.2	0.3	0.68	5	19.5	1.1
Weighted average ± SD																	22.3	2.0
41/01-1	1	0.327	1.6	1.524	2.1	0.006	45.4	3.368	1.4	2.4	1157.0	0.21	17.3	0.4	0.81	5	21.3	1.1
41/01-2	1	0.109	1.7	0.951	2.0	0.005	32.7	1.615	1.4	2.4	1264.2	0.11	13.6	0.3	0.74	5	18.3	1.0
41/01-3	1	0.081	1.7	0.923	2.1	0.002	33.2	1.833	1.4	2.4	1194.9	0.09	16.0	0.4	0.83	5	19.3	1.0
41/01-4	1	0.066	1.8	1.176	2.1	0.002	46.1	2.286	1.4	2.5	1707.6	0.06	15.8	0.4	0.77	5	20.4	1.1
41/01-5	1	0.079	1.7	0.694	2.0	0.004	37.4	1.115	1.4	2.4	1261.1	0.11	12.8	0.3	0.80	5	16.1	0.9
Weighted average ± SD																	18.7	2.0
43/01-1	1	0.230	1.6	2.455	2.1	0.005	33.6	3.532	1.2	2.4	1643.1	0.09	11.6	0.3	0.73	5	15.8	0.8
43/01-2	1	0.840	1.6	1.888	2.0	0.002	24.0	2.619	1.2	2.2	1413.5	0.44	10.3	0.2	0.74	5	14.0	0.7
43/01-3	1	0.207	1.6	0.607	2.0	0.004	40.7	1.449	1.2	2.3	4648.3	0.34	18.2	0.4	0.83	5	21.9	1.2
43/01-4	1	0.119	1.7	0.671	2.1	0.004	39.7	0.760	1.2	2.3	555.4	0.18	8.9	0.2	0.73	5	12.3	0.7
43/01-5	1	0.336	1.6	1.280	2.0	0.001	35.5	2.617	1.2	2.3	1205.8	0.26	15.8	0.4	0.77	5	20.4	1.1
Weighted average ± SD																	15.4	4.1
T5-1	1	0.243	1.6	0.860	2.1	0.003	20.5	2.141	1.2	2.3	625.1	0.28	19.2	0.4	0.62	5	31.1	1.7
T5-2	1	0.835	1.6	0.363	2.1	0.024	5.5	1.734	1.2	1.9	637.5	2.29	25.5	0.5	0.67	5	38.0	2.1
T5-3	1	0.124	1.7	1.079	2.3	0.000	21.9	3.407	1.2	2.5	919.7	0.11	25.2	0.6	0.65	5	38.7	2.1
T5-4	1	0.095	1.7	0.681	2.1	0.005	58.0	2.398	1.2	2.3	781.2	0.14	28.0	0.6	0.68	5	41.2	2.2
T5-5	1	0.129	1.7	0.823	2.1	0.004	52.5	2.332	1.2	2.4	840.2	0.16	22.4	0.5	0.65	5	34.6	1.9
Weighted average ± SD																	36.0	3.9
T6-1	1	0.112	1.7	0.439	2.1	0.003	31.5	1.809	1.2	2.3	405.2	0.25	31.9	0.7	0.70	5	45.5	2.4
T6-2	1	0.052	1.9	0.531	2.1	0.009	39.1	2.522	1.2	2.3	701.9	0.10	38.1	0.9	0.72	5	52.9	2.8
T6-3	1	0.116	1.7	0.510	2.1	0.002	42.6	2.375	1.2	2.4	633.2	0.23	36.2	0.9	0.71	5	51.0	2.7
T6-4	1	0.218	1.6	0.974	2.1	0.002	62.7	2.651	1.2	2.3	1269.6	0.22	21.2	0.5	0.64	5	33.1	1.8
T6-5	1	0.193	1.6	0.620	2.0	0.002	22.5	2.455	1.2	2.2	990.6	0.31	30.3	0.7	0.69	5	43.9	2.4
Weighted average ± SD																	43.0	7.8

Table 2. (continued)

Zircon (U-Th-Sm)/He Data From Tatra Mountains

Sample Code	Nc	232Th (ng)	± (%)	238U (ng)	± (%)	147Sm (ng)	± (%)	He (ncc)	± (%)	TAU (%)	eU	Th/U	Raw Age (Ma)	±1σ (Ma)	Ft	± (%)	Cor. Age (Ma)	±1σ (Ma)
27/02-1	1	0.686	1.6	1.352	2.0	0.004	33.3	6.859	1.2	2.2	677.3	0.50	37.2	0.8	0.77	5	48.2	2.6
27/02-2	1	0.418	1.6	0.621	2.1	0.013	10.3	2.745	1.2	2.2	515.3	0.67	31.3	0.7	0.74	5	42.5	2.3
27/02-3	1	0.660	1.6	0.778	2.1	0.005	53.7	3.846	1.2	2.1	543.6	0.84	33.8	0.7	0.73	5	46.3	2.5
27/02-4	1	0.089	1.7	1.225	2.2	0.002	61.4	4.893	1.2	2.4	863.6	0.07	32.2	0.8	0.73	5	44.0	2.4
27/02-5	1	0.591	1.6	1.611	2.0	0.010	40.0	6.592	1.2	2.2	1800.2	0.36	30.9	0.7	0.72	5	43.2	2.3
Weighted Average ± SD																	44.6	2.3
28/02-1	1	0.136	1.7	1.984	2.2	0.002	16.0	7.753	1.4	2.5	633.2	0.07	31.5	0.8	0.74	5	42.4	2.3
28/02-2	1	0.162	1.6	1.473	2.0	0.009	31.9	5.987	1.4	2.4	523.5	0.11	32.5	0.8	0.76	5	42.7	2.3
28/02-3*	1	0.196	1.6	0.841	2.0	0.005	31.4	7.488	1.4	2.4	392.0	0.23	69.0	1.6	0.77	5	89.6	4.8
28/02-4*	1	0.192	1.6	1.585	2.1	0.005	32.7	10.141	1.4	2.5	800.7	0.12	50.9	1.3	0.74	5	69.2	3.7
28/02-5	1	0.097	1.7	0.892	2.0	0.003	27.6	3.144	1.4	2.4	552.5	0.11	28.2	0.7	0.74	5	38.0	2.0
Weighted average ± SD (fliers omitted)																	40.8	2.6
30/02-1	1	0.300	1.6	0.837	2.1	0.002	16.4	3.336	1.2	2.3	805.8	0.36	30.1	0.7	0.82	5	36.6	2.0
30/02-2	1	0.165	1.6	0.876	2.1	0.003	29.8	2.453	1.2	2.3	578.6	0.19	22.0	0.5	0.77	5	28.7	1.5
30/02-3	1	0.217	1.6	0.871	2.1	0.007	42.5	2.421	1.2	2.3	619.9	0.25	21.5	0.5	0.78	5	27.5	1.5
30/02-4	1	0.271	1.6	0.909	2.1	0.001	11.4	2.719	1.2	2.3	483.0	0.30	22.9	0.5	0.79	5	28.9	1.5
30/02-5	1	0.190	1.6	0.572	2.1	0.004	44.0	1.503	1.2	2.3	603.6	0.33	20.0	0.5	0.79	5	25.5	1.4
Weighted average ± SD																	28.6	4.2
32/02-1	1	0.382	1.6	0.681	2.1	0.003	16.7	2.709	1.2	2.2	1151.7	0.56	28.8	0.6	0.87	5	33.2	1.8
32/02-2	1	0.324	1.6	2.096	2.0	0.006	48.5	6.257	1.2	2.3	634.9	0.15	23.6	0.6	0.81	5	29.2	1.6
32/02-3	1	0.498	1.6	2.860	2.0	0.013	12.3	7.215	1.2	2.3	1458.2	0.17	19.9	0.5	0.80	5	25.0	1.4
32/02-4	1	0.193	1.6	2.992	2.0	0.004	27.4	10.370	1.2	2.4	966.7	0.06	28.0	0.7	0.82	5	34.1	1.8
32/02-5	1	0.417	1.6	1.721	2.0	0.002	31.8	5.976	1.2	2.3	1261.6	0.24	27.0	0.6	0.83	5	32.6	1.8
Weighted average ± SD																	30.0	3.8
38/02-1	1	0.114	1.7	1.036	2.1	0.004	37.7	2.748	1.4	2.4	820.5	0.11	21.2	0.5	0.73	5	28.9	1.5
38/02-2	1	0.595	1.6	0.978	2.0	0.004	23.6	3.924	1.4	2.3	537.3	0.60	28.8	0.6	0.74	5	38.9	2.1
38/02-3	1	0.310	1.6	1.191	2.0	0.007	28.9	4.381	1.4	2.4	608.7	0.26	28.4	0.7	0.74	5	38.2	2.0
38/02-4	1	0.529	1.6	1.401	2.0	0.003	13.9	3.514	1.4	2.3	799.5	0.38	18.9	0.4	0.72	5	26.4	1.4
Weighted average ± SD																	31.3	6.4
39/02-1	1	0.256	1.6	1.810	2.0	0.004	38.6	5.405	1.2	2.3	1066.1	0.14	23.7	0.5	0.68	5	34.7	1.9
39/02-2*	1	0.260	1.6	0.415	2.1	0.004	19.0	7.765	1.2	2.2	189.0	0.62	132.4	2.9	0.62	5	212.6	11.4
39/02-3	1	0.167	1.6	1.796	2.1	0.001	21.7	4.610	1.2	2.4	899.0	0.09	20.6	0.5	0.65	5	31.8	1.7
39/02-4	1	1.092	1.6	1.672	2.0	0.021	17.6	4.898	1.2	2.1	885.6	0.65	20.8	0.4	0.66	5	31.4	1.7
39/02-5	1	0.140	1.6	0.479	2.1	0.007	24.8	1.022	1.2	2.3	386.5	0.29	16.4	0.4	0.65	5	25.3	1.4
Weighted average ± SD (fliers omitted)																	29.9	3.9
47/02-1	1	0.507	1.6	2.967	2.0	0.006	31.1	4.939	1.4	2.4	932.2	0.17	13.1	0.3	0.67	5	19.5	1.1
47/02-2	1	0.300	1.6	1.284	2.0	0.007	36.7	3.325	1.4	2.4	791.6	0.23	20.1	0.5	0.76	5	26.5	1.4
47/02-3	1	0.858	1.6	1.288	2.0	0.017	30.5	2.348	1.4	2.3	540.9	0.66	12.9	0.3	0.70	5	18.6	1.0
47/02-4	1	0.893	1.6	2.946	2.1	0.012	13.6	4.957	1.4	2.4	1510.8	0.30	12.9	0.3	0.69	5	18.7	1.0
47/02-5	1	0.543	1.6	1.866	2.1	0.005	11.2	2.432	1.4	2.4	1158.2	0.29	10.0	0.2	0.65	5	15.3	0.8
Weighted average ± SD																	18.6	4.1

[a]^{4}He: volume of ^{4}He in ncc at standard temperature and pressure; TAU: total analytical uncertainty; Unc. age: uncorrected (U-Th)/He age; Ft: alpha retention factor after *Farley et al.* [1996]; Cor. age: (U–Th)/He age corrected for alpha ejection.

ZHe age (18.7 ± 2.0 Ma), documenting a long gap between the closure of the two thermochronometers. This Early Eocene age is younger than the Paleocene ZFT ages of ~77–63 Ma reported by *Králiková et al.* [2014] from the SE margin of the Tatra Mountains (Figure 3a).

A summary of ZHe results is presented in Table 2 and Figures 3a–3c and 4. Seventy-six single grain ZHe ages determined for 16 basement samples range from 50.4 ± 7.3 Ma to 15.4 ± 4.1 Ma, with the majority clustering between ~40 and ~20 Ma. These ages are similar to ZHe ages of ~44–21 Ma reported by *Śmigielski et al.* [2010, 2011, 2012]. Reproducibility of replicates (typically five per sample) is very good in nearly all samples. Only sample 39/02 revealed one anomalously old ZHe age of 212.6 ± 11.4 Ma. While we acknowledge that such

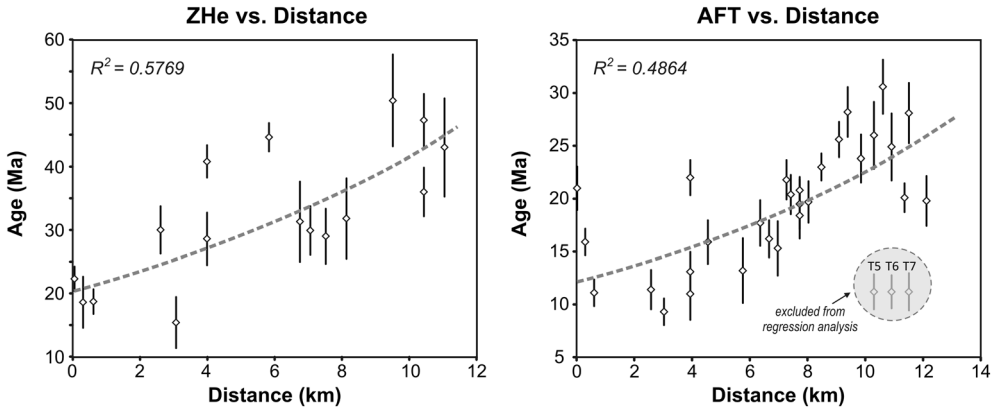

Figure 4. (left) ZHe and (right) AFT ages from this study plotted as a function of the distance from Sub-Tatra fault, where a reasonably good trend of ages increasing away from the major fault is visible. The trend lines represent exponential regression curves calculated using Excel. For regression analysis of AFT data we omitted three samples (T5, T6, and T7) from the locally rejuvenated basement block in the central northern part of the Tatra Mountains, which are clearly "detrended."

an anomalously old age may have represented a highly retentive crystal that was not reset by the Alpine overprint, we consider it to be an analytical outlier and reject this age from further considerations, because the remaining grains form a relatively tight cluster of much younger ZHe ages (25 to 35 Ma).

In a map view, ZHe ages show a discernible spatial pattern (Figures 3a and 4) where the older (Eocene-Oligocene) ages (~50–29 Ma) are found in the central part of the range, whereas the younger (Miocene) ages (22–15 Ma) are located exclusively along or close to the southern margin of the range in the vicinity of the Sub-Tatra fault, suggesting its activity at that time. It is also evident that ZHe ages in the central western part (50–40 Ma) are older than those in the central eastern part of the range (43–29 Ma), implying a segmentation of the basement into smaller blocks that underwent differential cooling history in the Cenozoic (Figure 3b). Four samples from the steep elevation profile on the Rysy Peak range from ~32 to 29 Ma, but only the two topmost samples show a positive correlation with altitude (Figure 2b).

4.2. AFT Data

Results of AFT analysis are presented in Table 1 and Figures 2b, 2c, 3a, 3d, 3e, and Figures S1 and S2 in the supporting information. All but two samples consist of a single age population as shown by high $P(\chi^2)$ values (Table 1). The two samples—a Triassic sandstone (9/01) in the NW part and a metamorphic schist (T3) in the western central part revealed a large spread of single grain ages (from Eocene to Miocene and Early Miocene to Late Miocene, respectively) that failed the $P(\chi^2)$ test and a suggested complex cooling history. Chlorine content determined by electron microprobe (EMP) in these and other six samples (9/01, 14/01, T3, T5, T6, and 30/02) was found to be $<$0.1 wt % in all analyzed crystals, and therefore, chemical variations do not account for the age variations. Measured Dpar values (~1.5 μm in average; Table 1) are in the range of Durango apatite [*Ketcham et al.*, 2007], indicating fluorine-rich apatite composition, which agrees with the composition determined by EMP.

AFT ages range from 30.6 ± 2.6 to 9.3 ± 1.3 Ma and point to an Oligocene-Miocene cooling. All AFT ages are younger or overlap within uncertainty with the corresponding ZHe ages, which is in agreement with the closure temperature concept [*Dodson*, 1973]. AFT ages from the basement rocks in the western and eastern parts of the Tatra Mountains do not show any significant difference. AFT ages from the Tatric sedimentary cover (8/01, 9/01) are younger than their Triassic stratigraphic age, pointing to a post-depositional resetting at temperatures of $>$110°C. Lower Oligocene sandstone (38/01) from the CCPB located south of Sub-Tatra fault with an age of 22.2 ± 3.1 Ma is also reset suggesting postdepositional heating to $>$110°C.

Track lengths were measured in 30 samples (Figure S2); however, due to young AFT age and the relatively low uranium content in apatite, typically only about 20 track lengths could be measured per sample and only in three samples (14/01, 27/01, and 39/02) were we able to measure over 50 confined tracks. Given the low number of confined tracks measured in majority of our samples, the observed patterns of track length

distribution should be interpreted with caution. Track length distributions vary from broad bimodal patterns, through broad unimodal to narrow unimodal patterns, suggesting a variety of cooling styles for different samples. Mean track lengths for all but one sample range from 11.1 to 13.6 μm, which is typical for a complex or a moderate cooling through the apatite partial annealing zone (PAZ ~60–120°C) [e.g., *Wagner and Van den Haute*, 1992].

In general, our new AFT results are in good agreement with majority of the published AFT and apatite (U-Th)/He data that suggest an Oligocene-Miocene cooling [*Anczkiewicz et al*., 2005; *Baumgart-Kotarba and Kráľ*, 2002; *Burchart*, 1972; *Kráľ*, 1977; *Králiková et al*., 2014; *Struzik et al*., 2002; *Śmigielski et al*., 2010, 2011, 2012]. The only exceptions that are not considered for interpretation include the following: the 37 Ma age for an amphibolite in the northern part of the Tatra Mountains reported by *Burchart* [1972] (i.e., Burchart's sample 17), which we dated at 20.1 ± 1.4 Ma for a locality few meters away; and the 7–2 Ma AFT ages, reported by *Baumgart-Kotarba and Kráľ* [2002] from along the Sub-Tatra fault, which were dated by population method but could be confirmed neither by our AFT data nor by apatite (U-Th)/He data [*Śmigielski et al*., 2010, 2011, 2012]. In addition, it may also appear that four AFT ages of 13 ± 2 [*Burchart*, 1972, sample 1], 10 ± 2, 15 ± 2, and 15 ± 2 Ma [*Kráľ*, 1977] (samples ZK-2 to ZK-4) from the NW part of the range and obtained by population method, are questionable because all our ages from this region are significantly older (>25 Ma). However, our samples were collected at higher altitudes (>1800 m asl) and the four samples of *Burchart* [1972] and *Kráľ* [1977] were collected in valleys at lower altitudes (1250–1370 m asl), so their ages may record the same exhumation event recorded by deeper levels of the basement or a younger exhumation event related to valley incision. Hence, these ages are included for the purposes of the interpretation.

Spatial distribution of the cleaned AFT data shows an ill-defined S/SE ward younging trend (Figures 3a–3e), which is more visible in the western part of the range. The oldest ages of 30–23 Ma are found in the northern and western parts of the crystalline basement; the intermediate ages of 23–16 Ma are located more to the south and SE of the first zone. The youngest ages of 16–8 Ma are found in the southern margin of the massif close to the Sub-Tatra fault (Figures 3 and 4), but locally also in other parts of the Tatra Mountains (e.g., NW part of the eastern segment) where they occur in the vicinity of shear zones and minor faults (samples T5, T6, and T7), or at valley bottoms (e.g., our sample 34/02 or the samples of *Kráľ* [1977] discussed in the previous paragraph) (Figure 2a).

We found a positive correlation between our AFT ages and their distance from the major fault (Figure 4); however, this trend became less clear when AFT data from older studies [*Burchart*, 1972; *Kráľ*, 1977] were included, but were confirmed by modern data of *Králiková et al*. [2014]. AFT ages from the steep elevation profile show an offset likely related to a fault (Figure 2b). The slope of linear regression for the topmost three samples suggests an exhumation rate of ~200 m/Myr.

5. Thermal History Modeling

In order to achieve the best possible parameterization of the model, the thermal history was modeled only for those samples for which ZHe, AFT age, and track length data were available. The objectives of the modeling were as follows: (i) to estimate maximum posttectonic burial temperatures in the Paleogene that can be approximated by ZHe data and (ii) to define the timing and rate of final cooling that is constrained by AFT data. Based on the current geologic knowledge of the evolution of the Tatra Mountains and surrounding areas, the model was constrained as follows:

The starting point of the time-temperature (tT) path for basement samples was set as $T = 350–250$°C at ~100–80 Ma, which marks the thermal maximum during tectonic burial during the Eo-Alpine nappe stacking in the Late Cretaceous (Turonian) as documented by the reset $^{40}Ar/^{39}Ar$ system in mica [*Dallmeyer et al*., 1993, 1996; *Maluski et al*., 1993; *Moussallam et al*., 2012]; closure temperature of Ar/Ar system based on *McDougall and Harrison* [1988]. For sediment sample (47/02) the starting point was set at $T = 200–150$°C, at ~100–80 Ma, according to the Eo-Alpine thermal maximum estimated from paleomagnetic data [*Grabowski et al*., 1999; *Kotarba*, 2003; *Lefeld*, 1997; *Środoń et al*., 2006; *Wolska et al*., 2002].

During postorogenic collapse in the early Paleogene, the basement complex with the Mesozoic nappe stack was exhumed and the Mesozoic nappes across the entire range as well as some parts of the crystalline basement in the western Tatra Mountains were exposed to erosion as late as ~50 Ma (prior to the CCPB

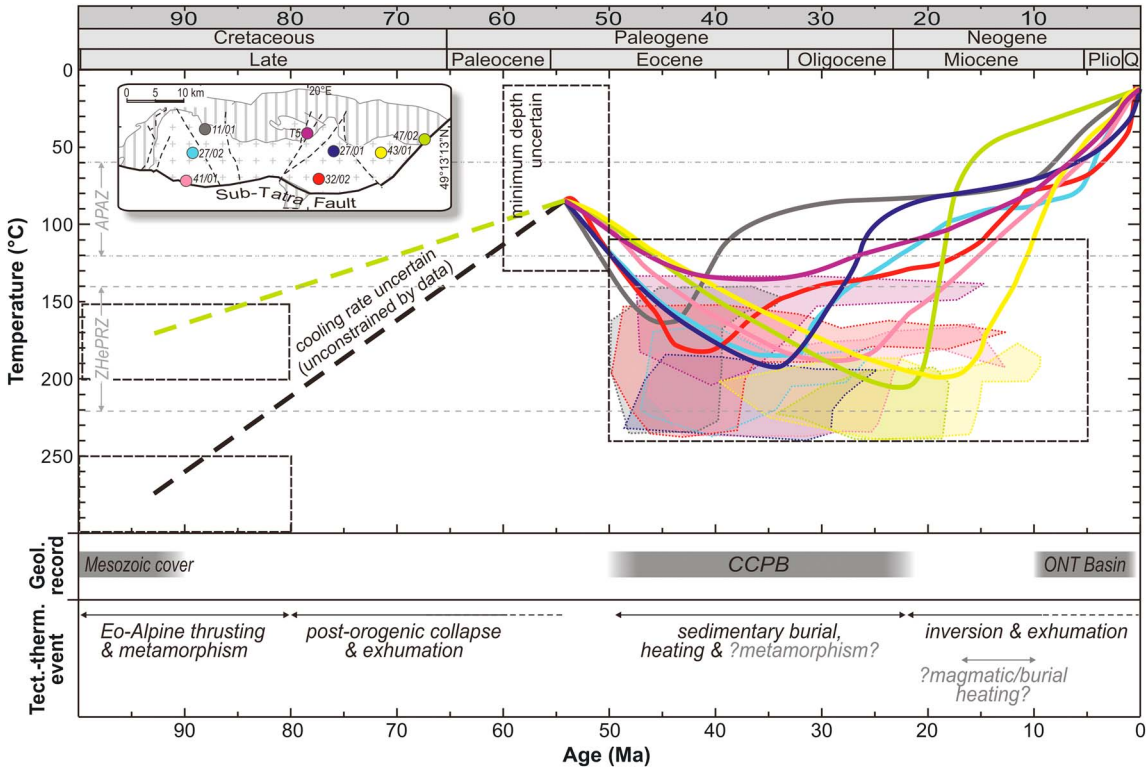

Figure 5. (top) Time-temperature diagram showing superimposed good fit thermal trajectories of the samples modeled by HeFTy [*Ketcham*, 2005]. Colored thick lines (color coded according to the samples in the inset) represent weighted mean cooling path based on good fit trajectories, where a "good" result corresponds to the "Goodness-of-Fit" value of 0.5 or higher. Shaded polygons (color coded according to the samples in the inset) show the plausible values of peak temperatures during CCPB burial; dashed rectangles represent constraints defined according to available geological record (see the text for details). Thick black dashed line, representing the exhumation related to the Late Cretaceous-Early Eocene postorogenic collapse, is not constrained by thermochronological data and is assumed to be identical for all samples based on geological arguments (see the text for details). ZHe PRZ: ZHe partial retention zone; APAZ: apatite partial annealing zone. (middle) Available geological record in the Tatra Mountains and surrounding basins. ONT: Orava-Novy Targ Basin. (bottom) Major tectonothermal events in the Central Western Carpathians. On Figure 5 (top) note (i) the increase in maximum temperature, (ii) the "delay" in the onset of final exhumation, and (iii) the increase in cooling rate of the last cooling phase with decreasing distance to the Sub-Tatra fault.

transgression), as evidenced by Triassic and Liassic clasts in the basal conglomerate of Nummulitic Eocene succession [*Andrusov*, 1959; *Lefeld*, 1985, 1997; *Lefeld et al*., 1985; *Nemčok and Nemčok*, 1994; *Roniewicz*, 1969]. However, there is little information on minimum temperatures and depths for other parts of the crystalline basement (especially the eastern Tatra Mountains) during the final stage of this exhumation stage, other than (i) cooling below ~240°C and 180°C constrained by some Late Cretaceous-Paleocene ZFT and ZHe ages, respectively [*Králiková et al*., 2014; *Śmigielski et al*., 2012], and (ii) the thickness of the cover nappes did not likely exceed 4 km in total [*Nemčok et al*., 1993] corresponding to 90–130°C (unless stated otherwise, here and below we assume a paleogeothermal gradient of 20–30°C/km and surface temperature of 10°C). Therefore, we set a wide temperature constraint of $T = 130–10$°C at 60–50 Ma.

In the Eocene at 49–42 Ma (Lutetian), sea transgraded the area and the Tatra Mountains may have been subsequently buried under the Eocene-lowermost Miocene sediments, the thickness of which could have exceeded 4 km as estimated from the CCPB record in surrounding basins [*Garecka*, 2005; *Gedl*, 2000; *Marschalko*, 1968; *Olszewska and Wieczorek*, 1998; *Soták et al*., 2001; *Starek*, 2001] and from the reset AFT and ZHe ages. The maximum temperatures, however, did not exceed ~240°C (closure temperatures of ZFT system) [*Brandon et al*., 1998] as the ZFT ages were not fully reset (this study) [*Králiková et al*., 2014]. CCPB sedimentary succession in the basins surrounding the Tatra Mountains terminated in the early Miocene, so the burial could have lasted until then. However, it is possible that the younger Miocene sediments may have been eroded away later. Therefore, we set a constraint of $T = 240–110$°C at 49–15 Ma. The onset of final exhumation likely varied across the range as given by the broad range of AFT ages and, accordingly, could

have started as soon as in the Oligocene in the north and as late as in the Miocene in the south. We did not impose any constraint on this period. The end of the tT path was set to $T = 10$°C at 0 Ma according to the present-day annual mean surface temperature.

The modeling results for individual samples can be found in the supporting information (Figure S3) with a summary shown in Figure 5. The common feature for all the modeled tT paths is the peak temperatures of >150°C (approximately the lower temperature limit of the zircon He partial retention zone (ZrHePRZ), ca. 140–220°C) [*Guenthner et al*., 2013] that followed the Paleocene-early Eocene cooling. However, the magnitude of the thermal peak and the timing of the onset of the cooling following this thermal peak vary for different parts of the Tatra Mountains The modeled thermal peaks (Figure 5) form a distinct spatial trend, which intrinsically correlates with the spatial pattern of ZHe and AFT ages and suggest a migration of the exhumation locus or burial depth from the north toward the south, or toward the major fault in the south. Samples from the central western and central eastern parts of the range (with Eocene and Oligocene ZHe ages, respectively, and Oligocene and Miocene AFT ages, respectively) could have cooled from the ZrHePRZ as early as in the latest Eocene but possibly only in the Early Miocene, before cooling through the partial annealing zone of the apatite fission track thermochronometer (APAZ; 120–60°C) at relatively slow rate (~1–5°C/Ma) in the Miocene. In contrast, samples with Miocene ZHe and AFT ages located in the south along the major fault left the ZrPRZ in the Miocene and cooled through the APAZ at high rate (~20°C/Ma).

6. Interpretation and Discussion

6.1. Tectonothermal History Reconstruction

6.1.1. Eo-Alpine Postorogenic Exhumation and Paleogene Burial

As expected from the resetting of higher-temperature thermochronometers such as the K-Ar and Ar-Ar systems (see section 2), the ZFT and ZHe thermochronometers were also reset during the Eo-Alpine nappe stacking [*Plašienka et al*., 1997]. This conclusively proves that the crystalline basement reached temperatures above ~240°C (closure temperatures of the ZFT system) [*Brandon et al*., 1998] and therefore experienced at least a very low-grade Eo-Alpine metamorphic overprint.

The early Eocene ages of 55.2 ± 4.3 Ma (ZFT; sample 41/01) and 50.4 ± 7.3 Ma (ZHe; sample 13/01) found in the western Tatra Mountains postdate the Alpine nappe stacking and predate the Paleogene burial. Together with latest Cretaceous ZFT ages from 76.8 ± 11 to 62.6 ± 6.0 Ma [*Králiková et al*., 2014] and $^{40}Ar/^{39}Ar$ ages (~75–50 Ma) on biotite and muscovite from the granitoids, mylonites, and pseudotachylytes [*Kohút and Sherlock*, 2003; *Maluski et al*., 1993], these ages might be interpreted as recording a cooling related to exhumation of the Tatra Mountains basement during the extensional collapse of the Carpathian orogenic wedge. Sample 13/01 remained at <180°C temperatures since exhumation, suggesting that the amount of the subsequent Paleogene overburden (see next paragraph) at this locality was smaller than that in other parts of the range. Alternatively, we speculate that our early Eocene ages could reflect partial resetting during the CCPB burial as explained in the next paragraph.

The majority of ZHe ages are clearly younger than ~50 Ma. The simplest interpretation would suggest that these ages record a protracted cooling of the basement through the ZHe partial retention zone (ca. 140–220°C) [*Guenthner et al*., 2013] related to exhumation, in the course of continuing extensional collapse of the orogenic wedge. This interpretation, favored by *Kováč et al*. [1994], may find support in good reproducibility of single grain ZHe ages (see Table 2) typical for quickly cooled samples [e.g., *Fitzgerald et al*., 2006]. However, given the strong geological evidence, such as (i) material derived from the Variscan basement and Mesozoic cover sequences found in the basal conglomerates of the CCPB, pointing to the near-surface position of the basement in the Paleocene (see sections 2 and 5) and (ii) the great thickness of existing and eroded CCPB sediments documented by a fully reset AFT age (22.2 ± 3.1 Ma) from the Lower Oligocene sandstone (sample 38/01; depositional age: 49–42 Ma), we believe that the Eocene-early Oligocene ZHe ages reflect partial or full resetting of the ZHe system caused by reheating of the basement by Paleogene sediment (Figures 3a–3c and 5). Given this explanation, we would like to emphasize that the Eocene-early Oligocene ZHe ages are "apparent" ages without any direct connection to a distinct cooling event and, as opposed to the traditionally adopted view, should not be seen as "cooling" ages.

The burial depth of the crystalline basement during the Eocene-Oligocene varied across the region: ZHe ages in the NW, easternmost, and southern parts of the Tatra Mountains vary from >40 Ma to 43–29 Ma and 15 Ma,

respectively. This spatial pattern suggest that the NW part of the Tatra Mountains was buried to shallower (or "colder") depths during the Paleogene burial and exhumed through the ZrPRZ earlier (possibly in the Early Oligocene) than in the eastern and southern parts, which cooled through the ZrPRZ in the Oligocene-middle Miocene (Figures 3a–3c and 5).

Burial depth can be calculated by conversion of the measured maximum temperatures provided the paleogeothermal gradient can be reasonably estimated. The fully reset AFT system (22.2 ± 3.1 Ma) in the Lower Oligocene sandstone (38/01) in the Liptov Basin south of Sub-Tatra fault suggests a postdepositional heating to >110°C, which corresponds to an overburden of at least 4–5 km (assuming a paleogeothermal gradient of 20–25°C/km assumed for relatively cold conditions typical for fore-arc basin environment) [*Dumitru*, 1991]. This estimate is in good agreement with the burial depths of 3–6 km based on fluid inclusion data [*Hurai et al*., 2002] and suggests that the original thickness of CCPB sediments was two times greater than the current thickness of ~3.5–5 km approximated from stratigraphic cross sections [*Soták et al*., 2001; *Starek*, 2001]. Full resetting of the AFT system in Paleogene sediments supports the significant depth and extent of the CCPB as has been reported from other parts of the Western Carpathians (e.g., in Podhale Basin or near Žiar Mountains.) [*Anczkiewicz et al*., 2013; *Danišík et al*., 2004, 2008a, 2008b, 2010, 2012] and is in agreement with burial depth estimates from vitrinite reflectance, fluid inclusion, and illite crystallinity data [*Hurai et al*., 2002; *Środoń et al*., 2006].

According to the ZHe data and the modeling results (Figure 5), the burial temperatures for the crystalline basement and its Triassic sedimentary cover must have exceeded ~150°C. We speculate that the basement likely experienced another phase of very low-grade metamorphism related to sedimentary burial, which is the first report of its kind (i.e., burial-related metamorphism of Paleogene age) from the Western Carpathians and should have implications for a redefinition of regional geological units which is based on age and grade of metamorphism [*Plašienka et al*., 1997; http://www.met-map.uni-goettingen.de]. Since the modeled minimum values of peak temperatures vary from 150 to 180°C range (depending on crystal size, cooling rate, and radiation damage) [*Guenthner et al*., 2013; *Reiners et al*., 2004; *Shuster et al*., 2006], our conservative estimate for the corresponding minimum burial depths based on the 20–25°C/km paleogeothermal gradient is ~5–7 km. Maximum burial temperatures clearly did not exceed ~300°C as no Paleogene Ar-Ar ages have been reported for the basement rocks. The existing gap of ~180–300°C is yet to be explored by more zircon fission track data sensitive to this temperature range [*Brandon et al*., 1998] and remains open for future studies.

6.1.2. Oligocene-Miocene Exhumation

While the exhumation of the Tatra basement through the apatite partial annealing zone has been long believed to have taken place at 20–10 Ma as inferred from youngest AFT data [e.g., *Kováč et al*., 1994], the actual onset of the exhumation has not been adequately addressed. Only *Kohút and Sherlock* [2002] correctly pointed out that the Oligocene AFT ages of *Burchart* [1972] reported from the northern parts of the range are generally ignored in published exhumation models. These authors suggested that the exhumation started already in the Eocene-Oligocene as inferred from the Eocene-Oligocene Ar-Ar ages on pseudotachylytes from the faults genetically related to the Sub-Tatra fault, pointing to its activity at that time [*Kohút and Sherlock*, 2002, 2003].

Our thermal modeling results alone cannot conclusively constrain the exact timing of the cooling onset, because the modeled thermal trajectories allow inflection points of "heating-to-cooling" transition to be anywhere between the Middle Eocene and the Middle Miocene. However, based on the averages of good thermal trajectories modeled in the majority of samples (thick lines in Figures 5 and S3) and the fact that the inversion of the CCPB basin started in the Oligocene as inferred from structural and sedimentological data [e.g., *Nemčok*, 1993; *Sperner et al*., 2002], we favor the exhumation starting in the Oligocene.

The modeling results and spatial distribution of ZHe and AFT ages collectively suggest that the locus of exhumation migrated toward the south and that the rate and style of the final cooling also varied across the range in the same direction. This is in accord with the northward tilting and asymmetric exhumation of the Tatra Mountains expected from the geological record [*Bac-Moszaszwili et al*., 1984; *Jurewicz*, 2000; *Piotrowski*, 1978; *Sokołowski*, 1959; *Uhlig*, 1899]. In general, our results show that the northern and NW parts of the Tatra Mountains (with Oligocene and Early Miocene AFT ages of >20 Ma) that were buried to shallower depths during the Paleogene (see previous section) entered the apatite PAZ in the Oligocene and cooled at slow rates of ~1–5°C/Ma. In contrast, southern segments of the range (in some cases with almost identical

Miocene ZHe and AFT ages) along the major fault were exhumed from greater depths, entered the apatite PAZ later (i.e., in the Middle to Late Miocene), and cooled rapidly through it at rates of ~10–20°C/Ma. At a smaller scale, the observed variations in thermochronological data over short distances can be attributed to the segmentation of the basement by faults [*Bac-Moszaszwilli*, 1993; *Kohút and Sherlock*, 2002, 2003], which controlled their differential exhumation.

The cooling rates in the Miocene period cannot be straightforwardly converted into exhumation rates as the calculation depends on the selection of the paleogeothermal gradient. As shown in several works by *Danišík et al*. [2008a, 2008b, 2012, 2015], a "mid-Miocene thermal event" likely related to lithospheric thinning, asthenospheric diapir formation, magmatism, and/or sedimentary burial [*Dövényi and Horváth*, 1988; *Horváth and Royden*, 1981; *Stegena et al*., 1975; *Tari et al*., 1999] and characterized by elevated heat flow was responsible for partial and full resetting of AFT and AHe thermochronometers in several other crystalline cores of the IWC and in the neighboring Pannonian Basin. Given its widespread regional character, we believe that the '"mid-Miocene thermal event" not only increased the geothermal gradient in the study area during the Miocene but also could be responsible for partial resetting of the AFT thermochronometer documented by bimodal track length data observed in several samples. Therefore, conversion of modeled cooling trajectories into exhumation rates by adopting a value of 30°C/km, representing the increased geothermal gradient advocated here for the Miocene period, results in average exhumation rates in the order of 10–150 m/Myr and 300–600 m/Myr for the slowly cooled and rapidly cooled parts of the basement, respectively. However, since the real value of the Miocene paleogeothermal gradient has been determined in some parts of the Pannonian Basin [*Sachsenhofer et al*., 1997; *Sachsenhofer*, 2001] but nowhere near the study area, we emphasize that these numbers are likely biased by the chosen paleogeothermal gradient and should not be considered conclusive.

6.1.3. On Quaternary Exhumation

A few hundred meters of thick, gravel-dominated fluvial and glacial sediments of Quaternary age, deposited mostly at the southern foothills of the range and in the Orava-Nowy Targ Basin in the north [*Nemčok et al*., 1993; *Tokarski et al*., 2012], has been interpreted as indicating erosion related to accelerated uplift of the Tatra Mountains [*Tokarski et al*., 2012]. It was also argued that Pleistocene exhumation of the Tatra Mountains is recorded by some AFT ages [*Baumgart-Kotarba and Kráľ*, 2002]. Our AFT ages do not record any accelerated cooling in the Quaternary, proving that Quaternary erosion, despite being important in the formation of present-day topography, did not exceed 3 km. Apatite (U-Th)/He, apatite $^{4}He/^{3}He$ thermochronology [*Shuster and Farley*, 2005], or optically stimulated luminescence thermochronology [*Herman et al*., 2010] with lower closure temperatures than AFT system should better resolve this part of the cooling history and remains open for future studies.

6.2. Implications for the Activity of the Sub-Tatra Fault

It has been recognized more than 100 years ago that uplift and exhumation of the Tatra Mountains was accommodated by the W-E trending Sub-Tatra fault, which separates the Tatra horst from the CCPB sediments of the Liptov Basin in the south [*Uhlig*, 1899]. However, despite its crucial importance, not only for the genetic models of the Tatra Mountains exhumation but also for the tectonic regime in the northern CWC, the geometry, kinetics, amount of displacement, and timing of the fault's activity remain controversial [e.g., *Andrusov et al*., 1973; *Bielik et al*., 2004; *Castelluccio et al*., 2015; *Hrušecký et al*., 2002; *Kohút and Sherlock*, 2003; *Lefeld*, 2009; *Maheľ*, 1986; *Petrík et al*., 2003; *Sperner*, 1996; *Sperner et al*., 2002]. The Sub-Tatra fault is a polygenetic fault system, consisting of several segments that experienced complex tectonic evolution dominated by strike- and oblique-slip movements [*Bac-Moszaszwilli*, 1993; *Sperner*, 1996; *Sperner et al*., 2002]. Two opposite theories on the fault geometry have been put forward: According to some authors [e.g., *Biely and Fusán*, 1967; *Kotański*, 1961; *Lefeld*, 2009; *Nemčok et al*., 1993; *Sperner*, 1996; *Sperner et al*., 2002], the Sub-Tatra fault is a north dipping reverse fault and the Tatra Mountains were exhumed as a hanging wall along the back thrust in the compressional regime as inferred from structural data and field observations. In contrast, inferring from structural data, field observations, shallow seismic and drilling survey in Liptov Basin, some authors argued for a vertical or steep (65–90°), south dipping normal fault and exhumation of the Tatra Mountains as a footwall in an extensional regime [*Gross et al*., 1980; *Hrušecký et al*., 2002; *Jurewicz*, 2005, 2007; *Jurewicz and Bagiński*, 2005; *Kohút and Sherlock*, 2003; *Maheľ*, 1986; *Petrík et al*., 2003]. Our data do not provide any direct evidence on the geometry of the fault; however, they do provide important constraints on the timing and amount of displacement along the Sub-Tatra fault.

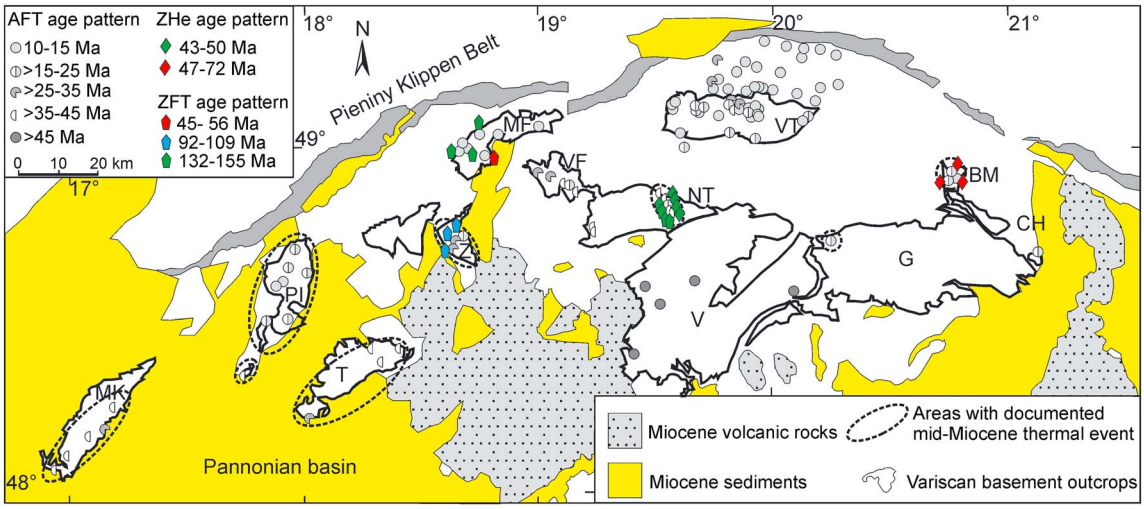

Figure 6. Simplified map of the Variscan crystalline outcrops (modified after *Lexa et al.* [2000]) and existing AFT, ZFT, and ZHe data, where AFT ages show a clear younging trend toward the former plate boundary (Pieniny Klippen Belt). Note that in several places with pre-Miocene AFT ages, the Miocene thermal event [*Danišík et al.*, 2011] has been reported. AFT data are compiled from the following studies: *Anczkiewicz et al.* [2005, 2013]; *Baumgart-Kotarba and Král'* [2002]; *Burchart* [1972]; *Danišík et al.* [2004, 2008a, 2008b, 2009, 2010, 2011]; *Král'* [1977]; *Kováč et al.* [1994]; *Struzik et al.* [2002]. ZFT data are from the following studies: *Danišík et al.* [2008b, 2010, 2011]. ZHe data are from *Danišík et al.* [2011, 2012]. Abbreviations: BM: Branisko Mountains, CH: Čierna Hora Mountains, G: Gemeric superunit, MF: Malá Fatra Mountains, MK: Malé Karpaty Mountains, NT: Nízke Tatry Mountains, PI: Považský Inovec Mountains, T: Tribeč Mountains, V: Veporic superunit, VF: Veľká Fatra Mountains, VT: Vysoké Tatry Mountains, Z: Žiar Mountains.

Based on the AFT data from the 1970s, it has been generally accepted that the Sub-Tatra fault was active in the Miocene (20–10 Ma), and accordingly, the amount of exhumation is typically estimated as ~5 km based on a conservative paleogeothermal gradient value of 20–25°C/km (see the previous section) [e.g., *Andrusov et al.*, 1973; *Burchart*, 1972; *Král'*, 1977; *Sperner*, 1996; *Sperner et al.*, 2002]. Recently, *Králiková et al.* [2014] argued for a much tighter Middle/early Late Miocene (9.3 ± 1.6 to 11.7 ± 1.8 Ma) span for the exhumation in the Slavkovský Peak area. In contrast, *Kohút and Sherlock* [2003] argued for the commencement of the Sub-Tatra fault activity already in the Oligocene (36–28 Ma) as based on Ar-Ar data on pseudotachylytes.

Our Miocene ZHe and AFT ages in combination with thermal modeling results for the samples collected in the vicinity of the Sub-Tatra fault zone (39/01, 40/01, 41/01, 33/02, 32/02, and 47/02) confirms that exhumation was active in the Miocene (23–9 Ma); however, the amount of exhumation is ~6 km when assuming the higher value of 30°C/km for paleogeothermal gradient (see above) or 9 km when assuming the more conventional value of 20–25°C/km for the paleogeothermal gradient. In either case, this amount of exhumation is significantly greater than previously thought. It is noteworthy that this high amount of Miocene exhumation was also documented by sample 47/02 in the easternmost segment of the Sub-Tatra fault (so-called Ružbachy fault), suggesting an en bloc exhumation of the Tatra Mountains basement along the whole distance of the Sub-Tatra fault.

Finally, as mentioned previously, our AFT data and thermal modeling results suggest that the final exhumation in some parts of the Tatra Mountains started in the Oligocene, which supports the Oligocene activity of the Sub-Tatra fault during the CCPB sedimentation as proposed by *Kohút and Sherlock* [2002, 2003].

6.3. Regional Correlation With Other Crystalline Cores and Surrounding Areas

It is noteworthy that similar AFT ages with both young (Miocene) and old (Oligocene) populations have been reported from the Podhale-Spišská Magura region [*Anczkiewicz et al.*, 2013] located to the north from our study area (Figure 6). The AFT ages in the eastern part of the Podhale-Spišská Magura Basin are in range of ca. 13–7 Ma like most of the Tatra Mountains, whereas in the western part of the basin the AFT ages are older (~30 Ma) similar to those in the western Tatra Mountains, suggesting a common thermal evolution for both areas.

From a broader regional perspective, our new data complement the existing pattern of low-temperature thermochronological data in the Western Carpathians [cf. *Danišík et al*., 2011] but provide additional complexities as explained below.

Based on current understanding, AFT ages from the crystalline core mountains show a clear younging trend toward the former plate boundary (Pieniny Klippen Belt), whereby the internal massifs retain mostly Palaeogene or Cretaceous AFT ages. All the external massifs (including the Tatra Mountains, Branisko Mountains, Malá Fatra Mountains, and northern Považský Inovec Mountains) show almost exclusively Miocene AFT ages, pointing to their residence in a relatively "hotter" environment (i.e., $> \sim 110$°C) in the Tertiary as compared to the internal massifs [cf. *Danišík et al*., 2011]. Given this seemingly clear spatial pattern, it has been speculated that the Oligocene AFT ages reported from the Tatra Mountains by *Burchart* [1972] were incorrect and should be ignored. However, our results confirmed that Oligocene AFT ages are indeed present in the northern parts of the Tatra Mountains.

Our Eocene ZFT and ZHe ages are almost identical with ZFT and ZHe ages reported from other crystalline complexes in the IWC (i.e., Tribeč Mountains, Malá Fatra Mountains, Nízke Tatry Mountains, Považský Inovec Mountains, Malé Karpaty Mountains, and Rochovce, Branisko Mountains) [*Danišík et al*., 2008b, 2010, 2011], revealing the Eo-Alpine metamorphic overprint and similar postcollisional tectonothermal evolution with the Paleogene burial (Figure 6). However, the Early to Middle Miocene ZHe ages found along southern parts of the Tatra Mountains are the youngest ZHe ages ever reported from a crystalline basement complex in the Western Carpathians. This supports the Tatra Mountains basement having experienced the deepest burial by CCPB sediments and the greatest amount of Miocene exhumation relative to any other crystalline core mountains in the Western Carpathians.

7. Conclusions

New ZFT, ZHe, and AFT data revealed a complex thermal evolution of the Tatra Mountains and provide further constraints on the Cenozoic geodynamic evolution of the Western Carpathians. The most important findings are the following:

1. As recorded by fully reset ZFT and ZHe ages, the crystalline basement was heated to temperatures above 240°C and therefore experienced at least a very low grade metamorphic overprint during the Eo-Alpine collision;
2. The vast majority of ZHe ages (~49–19 Ma) were reset at temperatures in excess of 150°C during the burial of the previously exhumed basement by CCPB sediments in the Middle Eocene-early Miocene, suggesting an overburden of at least 5–9 km for a large portion of the Tatra Mountains basement. The basement therefore experienced another very low grade metamorphic overprint. To our knowledge, this is the first report of burial-related metamorphism of Paleogene age in the Western Carpathians, which should have implications for regional reclassification of metamorphic units;
3. Oligocene-Miocene ZHe and AFT ages of 32–11 Ma record cooling during the final exhumation of the Tatra Mountains, related to lateral extrusion and rotation of the Tatra Mountains. The differences in the ZHe and AFT data over short distances are interpreted as the result of a variable burial depth and differential exhumation associated with block faulting;
4. Regional distribution of thermochronological data suggests an asymmetric exhumation starting in the NW at ~30–20 Ma at generally lower rates (~1-–5°C/Ma) and propagating to the SE toward the Sub-Tatra fault and Ružbachy fault, cooling through the apatite PAZ at 16–9 Ma at faster rates (~10–20°C/Ma);
5. The Miocene ZHe ages are the youngest reported for a crystalline basement complex in the Western Carpathians, suggesting that among all Western Carpathian core complexes, the Tatra Mountains were buried to the greatest depths in the Paleogene-Early Miocene and experienced the greatest amount of Miocene exhumation;
6. Miocene ZHe and AFT ages found in the vicinity of the Sub-Tatra major fault confirm its activity during the Miocene (and likely earlier) but suggest twice as much accommodated exhumation (i.e., ~9 km) as previously thought, which may have implications for structural models of Tatra Mountains exhumation;
7. The AFT data showed no evidence of accelerated cooling during the Quaternary indicating that Quaternary erosion related to the formation of present-day topography did not exceed 3 km.

Acknowledgments
A.A.A. thanks C. Xiang and PAS IGS for financial support (National Natural Science Foundation of China, grant 41272161) and the Tatra National Park authorities (both Polish and Slovak sites) for the permission to collect samples in the Tatra National Park. M.D. thanks I. Dunkl for sharing PepiFLEX software for ICP-MS data reduction and P.J.J. Kamp for access to the (U-Th)/He laboratory and financial support. N.J. Evans is acknowledged for linguistic improvements of the manuscript. M. Kohút and an anonymous reviewer are thanked for coinstructive reviews; K. Schulmann and C. Faccenna are thanked for editorial handling.

References

Anczkiewicz, A. A., M. Zattin, and J. Środoń (2005), Cenozoic uplift of the Tatras and Podhale Basin from the perspective of the apatite fission track analyses, *Mineral. Soc. Poland Spec. Pap.*, *25*, 261–264.

Anczkiewicz, A. A., J. Środoń, and M. Zattin (2013), Thermal history of the Podhale Basin in the internal Western Carpathians from the perspective of apatite fission track analyses, *Geol. Carpathica*, *64*(2), 141–151.

Andrusov, D. (1959), *Geology of the Czechoslovakian Carpathians. II*, 1st ed., 375 pp., SAV Publ., Bratislava (in Slovak).

Andrusov, D. (1965), Aperçu générale sur la géologie des Carpathes occidentales, *Bull. Soc. Geol. Fr.*, *7*, 1029–1062.

Andrusov, D., J. Bystrický, and O. Fusán (1973), Outline of the structure of the West Carpathians, in *Guide Book, X Congress CBGA*, pp. 5–45, D. Štúr Institute of Geology, Bratislava.

Bac-Moszaszwili, M., and E. Jurewicz (2010), *Voyage in Tatras*, TPN, Zakopane (in Polish).

Bac-Moszaszwili, M., W. Jaroszewski, and E. Passendorfer (1984), On the tectonics of Czerwone Wierchy and Giewont area in the Tatra Mts., Poland [In Polish with English summary], *Ann. Soc. Geol. Pol.*, *52*, 67–88.

Bac-Moszaszwilli, M. (1993), Struktura zachodniego zakończenia masywu tatrzańskiego (Structure of the western termination of the Tatra Massif), *Ann. Soc. Geol. Pol.*, *63*, 67–193.

Baumgart-Kotarba, M., and J. Kráľ (2002), Young tectonic uplift of the Tatra Mts. (fission track data and geomorphological arguments), *Geologica Carpathica* 53: Proceedings of the XVII Congress of the Carpathian-Balkan Geological Association Bratislava, September 1th-4th 2002. Eletronic version.

Behrmann, J. H., S. Stiasny, J. Milicka, and M. Pereszlenyi (2000), Quantitative reconstruction of orogenic convergence in the northeast Carpathians, *Tectonophysics*, *319*, 111–128.

Bieda, F. (1959), Paleontologiczna stratygrafia eocenu tatrzańskiego i fliszu podhalańskiego (Palaeontological stratigraphy of the Tatra Eocene and of the Podhale Flysch), *Biul. Inst. Geol.*, *149*, 215–224.

Bieda, F. (1963), Duże otwornice eocenu tatrzańskiego (Larger Foraminifers of the Tatra Eocene), *Pr. Inst. Geol.*, *37*, 1–215.

Bielik, M., J. Šefara, M. Kováč, V. Bezák, and D. Plašienka (2004), The Western Carpathians—Interaction of Hercynian and Alpine processes, *Tectonophysic*, *393*, 63–86.

Biely, A. (1989), The geological structure of the west Carpathians, in *Evolution of the Northern Margin of Tethys, 2*, *Mim. Sot. Gtol. Fr.*, vol. 154, edited by M. Rakus, J. Dercourt, and A. Nairm, pp. 51–57, Paris.

Biely, A., and O. Fusán (1967), Zum Problem der Wurzelzonen der subtatrischen Decken, *Geol. Pr., Správy*, *42*, 51–64.

Birkenmajer, K. (1986), Stages of structural evolution of the Pieniny Klippen Belt, Carpathians, *Stud. Geol. Pol.*, *88*, 7–32.

Birkenmajer, K. (2009), Quaternary glacigenic deposits between the Biała Woda and the Filipka valleys, Polish Tatra Mts, in the regional context, *Stud. Geol. Pol.*, *132*, 91–115.

Brandon, M. T., M. K. Roden-Tice, and J. I. Garver (1998), Late Cenozoic exhumation of the Cascadia accretionary wedge in the Olympic Mountains, NW Washington State, *Geol. Soc. Am. Bull.*, *110*(8), 985–1009.

Burchart, J. (1968), Rubidium-strontium isochron ages of the crystalline core of the Tatra Mts., Poland, *Am. J. Sci.*, *266*, 895–907.

Burchart, J. (1972), Fission-track age determination of accessory apatite from the Tatra Mountains, Poland, *Earth Planet. Sci. Lett.*, *15*, 418–422.

Burda, J., A. Gawęda, and U. Klötzli (2013), U-Pb zircon age of the youngest magmatic activity in the High Tatra granites (Central Western Carpathians), *Geochronometria*, *40*(2), 134–144, doi:10.2478/s13386-013-0106-9.

Burtner, R. L., A. Nigrini, and R. A. Donelick (1994), Thermochronology of Lower Cretaceous source rocks in the Idaho- Wyoming thrust belt, *Am. Assoc. Pet. Geol. Bull.*, *78*, 1613–1636.

Castelluccio, A., B. Andreucci, M. Zattin, R. A. Ketcham, L. Jankowski, S. Mazzoli, and R. Szaniawski (2015), Coupling sequential restoration of balanced cross sections and low-temperature thermochronometry: The case study of the Western Carpathians, *Lithosphere*, doi:10.1130/L436.1.

Csontos, L. (1995), Tertiary tectonic evolution of the Intra-Carpathian area: A review, *Acta Vulcanol.*, *7*, 1–13.

Csontos, L., A. Nagymarosy, F. Horvath, and M. Kováč (1992), Tertiary evolution of the Intra-Carpathian area: A model, *Tectonophysics*, *208*, 221–241.

Dallmeyer, D., F. Neubauer, and M. Putiš (1993), $^{40}Ar/^{39}Ar$ mineral age controls for the Pre-Alpine and Alpine tectonic evolution of nappe complexes in the Western Carpathians, in *PAEWCR Excursion Guide Stará Lesná*, edited by P. Pitoňák and J. Spišiak, pp. 13–20, Banska Bistrica.

Dallmeyer, D., F. Neubauer, R. Handler, H. Fritz, W. Müller, D. Pana, and M. Putiš (1996), Tectonothermal evolution of the internal Alps and Carpathians: Evidence from $^{40}Ar/^{39}Ar$ mineral and whole-rock data, *Eclogae Geol. Helv.*, *89*, 203–227.

Danišík, M., I. Dunkl, M. Putiš, W. Frisch, and J. Kráľ (2004), Tertiary burial and exhumation history of basement highs along the NW margin of the Pannonian Basin—An apatite fission track study, *Austrian J. Earth Sci.*, *95/96*, 60–70.

Danišík, M., M. Kohút, I. Dunkl, L. Hraško, and W. Frisch (2008a), Apatite fission track and (U-Th)/He thermochronology of the Rochovce granite (Slovakia)—Implications for the thermal evolution of the Western Carpathian-Pannonian region, *Swiss J. Geosci.*, *101*, 225–33.

Danišík, M., M. Kohút, I. Dunkl, and W. Frisch (2008b), Thermal evolution of the Žiar Mountains basement (Inner Western Carpathians, Slovakia) constrained by fission track data, *Geol. Carpathica*, *59*, 19–30.

Danišík, M., M. Kohút, I. Dunkl, and W. Frisch (2009), Fission track thremochronometry of the Vel'ká Fatra Mts. (Inner Western Carpathians, Slovakia): Constraints on the Alpine tectonothermal evolution, *7th Meeting of the Central European Tectonic Studies Group* (*CETeG*), Hungary, 13th–16th May 2009, Abstracts.

Danišík, M., M. Kohút, I. Broska, and W. Frisch (2010), Thermal evolution of the Mala' Fatra Mountains (Central Western Carpathians): Insights from zircon and apatite fission track thermochronology, *Geol. Carpathica*, *61*, 19–27.

Danišík, M., J. Kadlec, C. H. Glotzbach, A. Weisheit, I. Dunkl, M. Kohút, N. J. Evans, M. Orvošová, and B. J. McDonald (2011), Tracing metamorphism, exhumation and topographic evolution in orogenic belts by multiple thermochronology: A case study from the Nízke Tatry Mts., Western Carpathians, *Swiss J. Geosci.*, *104*, 285–98.

Danišík, M., M. Kohút, N. J. Evans, and B. J. McDonald (2012), Eo-Alpine metamorphism and the 'mid-Miocene thermal event' in the Western Carpathians (Slovakia): New evidence from multiple thermochronology, *Geol. Mag.*, *149*, 158–171.

Danišík, M., L. Fodor, I. Dunkl, A. Gerdes, J. Csizmeg, M. Hámor-Vidó, and N. J. Evans (2015), A multi-system geochronology in the Ad-3 borehole, Pannonian Basin (Hungary) with implications for dating volcanic rocks by low-temperature thermochronology and for interpretation of (U-Th)/He data, *Terra Nova*, doi:10.1111/ter.12155.

Dodson, M. H. (1973), Closure temperature in cooling geochronological and petrological systems, *Contrib. Mineral. Petrol.*, *40*, 259–274.

Donelick, R. A., R. A. Ketcham, and W. D. Carlson (1999), Variability of apatite fission-track annealing kinetics: II. Crystallographic orientation effects, *Am. Mineral.*, *84*(9), 1224–1234.

Dövényi, P., and F. Horváth (1988), A review of temperature, thermal conductivity, and heat flow data from the Pannonian Basin, In The Pannonian Basin, in *A Study in Basin Evolution*, *Am. Assoc. of Petrol. Geol. Mem.*, vol. 45, edited by L. H. Royden and F. Horváth, pp. 195–233.

Dumitru, T. A. (1991), Effects of subduction parameters on geothermal gradients in forearcs, with an application to Franciscan Subduction in California, *J. Geophys. Res.*, *96*(B1), 621–641, doi:10.1029/90JB01913.
Dumitru, T. A. (1993), A new computer automated microscope stage system for fission-track analysis, *Nucl. Tracks Radiat. Meas.*, *21*, 575–580.
Dunkl, I. (2002), TRACKKEY: A Windows program for calculation and graphical presentation of fission track data, *Comput. Geosci.*, *28*(1), 3–12.
Evans, N. J., J. P. Byrne, J. T. Keegan, and L. E. Dotter (2005), Determination of uranium and thorium in zircon, apatite, and fluorite: Application to laser (U-Th)/He thermochronology, *J. Anal. Chem.*, *60*, 1159–1165.
Farley, K. A. (2002), (U-Th)/He dating: Techniques, calibrations, and applications, *Rev. Mineral. Geochem.*, *47*, 819–44.
Farley, K. A., R. A. Wolf, and L. T. Silver (1996), The effect of long alpha-stopping distances on (U-Th)/He ages, *Geochim. Cosmochim. Acta*, *60*, 4223–4229.
Fitzgerald, P. G., S. L. Baldwin, L. E. Webb, and P. B. O'Sullivan (2006), Interpretation of (U-Th)/He single grain ages from slowly cooled crustal terranes: A case study from the Transantarctic Mountains of southern Victoria Land, *Chem. Geol.*, *225*, 91–120.
Frisch, W., I. Dunkl, and J. Kuhlemann (2000), Post-collisional large-scale extension in the Eastern Alps, *Tectonophysics*, *327*, 239–265.
Galbraith, R. F. (1981), On statistical models for fission track counts, *Math. Geol.*, *13*(6), 471–438.
Galbraith, R. F., and G. M. Laslett (1993), Statistical models for mixed fission track ages, *Nucl. Tracks Radiat. Meas.*, *21*, 459–470.
Garecka, M. (2005), Biostratygraphy and paleoenvironment of the Podhale Paleogene (Inner Carpathians, Poland) in the light of palynological studies. Part I, *Stud. Geol. Pol.*, *117*, 69–154.
Gawęda, A. (1995), Geochemistry and Rb/Sr isochron age of pegmatites from the Western Tatra Mts, *Geol. Carpathica*, *46*, 95–99.
Gawęda, A., K. Szopa, and D. Chew (2014), LA-ICP-MS U-Pb dating and REE patterns of apatite from the Tatra Mountains, Poland as a monitor of the regional tectonomagmatic activity, *Geochronometria*, *41*(4), 306–314.
Gedl, P. (1999), The age of base and top of the Podhale Palaeogene flysch (Central Carpathians, Poland), based on dinocysts, *Bull. Polish Acad. Sci. Earth Sci.*, *47*, 77–102.
Gedl, P. (2000), Biostratygrafia i paleośrodowisko paleogenu Podhala w świetle badań palinospastycznych. Część I. (Biostratigraphy and Palaeogene [Inner Carpathians, Poland] in the light of palynological studies. Part I, *Stud. Geol. Pol.*, *117*, 69–154.
Gleadow, A. J. W. (1981), Fission track dating methods: What are the real alternatives?, *Nucl. Track*, *5*, 3–14.
Gleadow, A. J. W., I. R. Duddy, and J. F. Lovering (1983), Fission track analysis: A new tool for the evaluation of thermal histories and hydrocarbon potential, *Aust. Pet. Explor. Assoc. J.*, *23*, 93–102.
Grabowski, J. (1997), New paleomagnetic data from Fatricum and Hronicum in the Tatra Mts (Poland) further evidences for Cretaceous remagnetization in the Central West Carpathians, *Przegląd Geol.*, *45*, 1074.
Grabowski, J., K. Narkiewicz, and P. Poprawa (1999), First results of paleomagnetic and paleothermal (CAI) investigations of the highest Sub-Tatric units in the Polish Tatra Mts, *Przegląd Geol.*, *47*, 153–158.
Green, P. F. (1981), 'Track-in track' length measurements in annealed apatites, *Nucl. Tracks*, *5*, 12–18.
Gross, P., et al. (1980), *Geology of Liptov Basin*, pp. 1–242, GÚDŠ, Bratislava [in Slovak].
Gross, P., E. Köhler, and O. Samuel (1984), New lithostratigraphic classification of the Central Carpathians Paleogene [in Slovak], *Geol. Pr., Správy*, *81*, 103–17.
Gross, P., et al. (1993), *Geology of Southern and Eastern Orava*, pp. 1–319, Dionýz Štúr Inst. Geol., Bratislava [in Slovak].
Guenthner, W. R., P. W. Reiners, R. A. Ketcham, L. Nasdala, and G. Giester (2013), Helium diffusion in natural zircon: Radiation damage, anisotropy, and the interpretation of zircon (U-Th)/He thermochronology, *Am. J. Sci.*, *313*, 145–198, doi:10.2475/03.2013.01.
Herman, F., E. J. Rhodes, J. Braun, and L. Heiniger (2010), Uniform erosion rates and relief amplitude during glacial cycles in the Southern Alps of New Zealand, as revealed from OSL-thermochronology, *Earth Planet. Sci. Lett.*, *297*(1), 183–189.
Horváth, F., and L. Royden (1981), Mechanism for the formation of the intra-Carpathian basins: A review, *Earth Evol. Sci.*, *3*(4), 307–316.
Hrušecký, I., L. Pospíšil, and M. Kohút (2002), Geological interpretation of the reflection seismic profile 753/92, in *Hydrocarbon Potential of the Eastern Slovakian Basin and Adjacent Areas*, *Open File Rep.*, edited by I. Hrušecký, pp. 1–47, Geofond, Bratislava, [in Slovak].
Hurai, V., A. Świerczewska, F. Marko, A. Tokarski, and I. Hrušecký (2000), Paleofluid temperatures and pressures in Tertiary accretionary prism of the Western Carpathians, *Slovak Geol. Mag.*, *6*, 194–7.
Hurai, V., J. Kihle, J. Kotulová, F. Marko, and A. Świerczewska (2002), Origin of methane in quartz crystals from the Tertiary accretionary wedge and fore-arc basin of the Western Carpathians, *Appl. Geochem.*, *17*(9), 1259–1271.
Hurford, A. J. (1986), Cooling and uplift patterns in the Lepontine Alps South Central Switzerland and age of vertical movement on the Insubric fault line, *Contrib. Mineral. Petrol.*, *92*, 413–27.
Hurford, A. J., and P. F. Green (1983), The zeta age calibration of fission-track dating, *Isot. Geosci.*, *1*, 285–317.
Janák, M. (1994), Variscan uplift of the crystalline basement, Tatra Mts, Central Western Carpathians: Evidence from $^{40}Ar/^{39}Ar$ laser probe dating of biotite and P-T paths, *Geol. Carpathica*, *45*(5), 293–300.
Janák, M., P. J. O'Brien, V. Hurai, and C. Reuter (1996), Metamorphic evolution and fluid composition of garnet-clinopyroxene amphibolites from the Tatra Mountains, Western Carpathians, *Lithos*, *39*, 57–79.
Janák, M., V. Hurai, L. Lhudová, P. J. O'Brien, and E. E. Horn (1999), Dehydration melting and devolatilization during exhumation of high grade metapelites: The Tatra Mountains, Western Carpathians, *J. Metamorph. Geol.*, *17*, 379–395.
Jurewicz, E. (2000), Tentative reconstructions of the stress axes from the thrust-folding stage in the Tatra Mts. on the basis of slickensides in the granitoid core, southern Poland [In Polish with English summary], *Przegląd Geol.*, *48*, 239–246.
Jurewicz, E. (2005), Geodynamic evolution of the Tatra Mts. and the Pieniny Klippen Belt (Western Carpathians): Problems and comments, *Acta Geol. Pol.*, *55*(3), 295–338.
Jurewicz, E. (2007), Multistage evolution of the granitoid core in Tatra Mountains, in *Granitoids in Poland*, *AM Monogr.*, vol. 1, edited by A. Kozłowski and J. Wiszniewska, pp. 307–317, Warsaw Univ., Warsaw.
Jurewicz, E., and B. Bagiński (2005), Deformation phases in the selected shear zones within the Tatra Mts granitoid core, *Geol. Carpathica*, *56*, 17–28.
Jurewicz, E., and A. Kozłowski (2003), Formation conditions of quartz mineralization in the mylonitic zones and on the slickenside fault planes in the High Tatra granitoids, *Arch. Mineral.*, *54*, 65–75.
Kázmér, M., I. Dunkl, W. Frisch, J. Kuhlemann, and P. Ozsvárt (2003), The Palaeogene forearc basin of the Eastern Alps and the Western Carpathians: Subduction erosion and basin evolution, *J. Geol. Soc., London*, *160*, 413–428.
Ketcham, R. A. (2005), Forward and inverse modeling of low-temperature thermochronometry data, in *Low- Temperature Thermochronology: Techniques, Interpretations, and Applications*, *Rev. Mineral. Geochem.*, vol. 58, edited by P. W. Reiners and T. A. Ehlers, pp. 275–314, Mineral. Soc. Am., Geochem. Soc., Chantilly, Va.
Ketcham, R. A., A. Carter, R. A. Donelick, J. Barbarand, and A. J. Hurford (2007), Improved modeling of fission track annealing in apatite, *Am. Mineral.*, *92*, 799–810.

Kohút, M., and S. C. Sherlock (2002), Pseudotachylytes from the High Tatra Mts.—Evidences for late paleogene seismic/tectonic events. XVII, pp. 1–4, *Congress of Carpathian-Balkan Geological Association*, September 1st - 4th.
Kohút, M., and S. C. Sherlock (2003), Laser microprobe ^{39}Ar - ^{40}Ar analysis of pseudotachylyte and host-rocks from the Tatra Mountains, Slovakia: Evidence for late Paleogene seismic/tectonic activity, *Terra Nova*, *15*, 417–424.
Koszowska, E., A. Wolska, and J. Szulc (1998), Tuffaceous intercalations within the Middle Triassic carbonates of the Hronicum unit in the Western Tatra Mts., Poland, *Carpathian- Balkan Geological Association*, *XVI Congress*.
Koszowska, E., J. Szulc, and A. Wolska (2001), Middle Triassic tuffaceous intercalations within the Reifling beds of the Western Tatra Mts., Poland, *Mineral. Soc. Pol. Spec. Papers*, *19*, 88–91.
Kotański, Z. (1961), Tektogeneza i rekonstrukcja paleogeografii pasma wierchowego w Tatrach, *Acta Geol. Pol.*, *11*, 187–467.
Kotarba, M. (2003), Historia diagenezy illitu/smektytu w skałach ilastych Karpat Zachodnich (przekrój Kraków - Zakopane), PhD thesis, 198 pp., Institute of Geological Sciences, Polish Academy of Sciences.
Kováč, M., J. Kráľ, E. Márton, D. Plašienka, and P. Uher (1994), Alpine uplift history of the Central Western Carpathians: Geochronological, paleomagnetic, sedimentary and structural data, *Geol. Carpathica*, *45*, 83–96.
Kováč, M., et al. (2007), Badenian evolution of the Central Paratethys sea: Paleogeography, climate and eustatic sea level changes, *Geol. Carpathica*, *58*, 579–606.
Kráľ, J. (1977), Fission track ages of apatites from some granitoid rocks in West Carpathians, *Geol. Carpathica*, *28*, 269–276.
Králiková, S., R. Vojtko, L. Sliva, J. Minár, B. Fügenschuh, M. Kováč, and J. Hók (2014), Cretaceous-quaternary tectonic evolution of the tatra Mts (Western Carpathians): Constraints from structural, sedimentary, geomorphological, and fission track data, *Geol. Carpathica*, *65*(4), 307–326.
Krist, E., S. P. Korikovsky, M. Putiš, M. Janák, and S. W. Faryad (1992), *Geology and Petrology of Metamorphic Rocks of the Western Carpathian Crystalline Complexes*, 324 pp., Comenius Univ. Press, Bratislava.
Książkiewicz, M. (1977), Tectonics of the Carpathians, in *Geology of Poland*, *Tectonics*, vol. IV, edited by W. Pożaryski, pp. 476–604, Wydawnictwa Geologiczne, Warszawa, Poland.
Lefeld, J. (1985), Main Geotraverse of the Polish Carpathians (Cracow-Zakopane), pp. 67–99. *Guide to excursion 2*, third day, Carpatho-Balkan Geological Association, XIII Congress, Cracow. Geological Institute, Poland.
Lefeld, J. (1997), Tektogeneza Tatr-Cykl alpejski, in *Guidebook of 68 Conference of the Polish Geological Society* [In Polish], pp. 16–21, Zakopane.
Lefeld, J. (2009), Alpine orogenic phases in the Tatra Mts [in Polish with English summary], *Przegląd Geol.*, *57*, 669–673.
Lefeld, J., A. Gaździcki, A. Iwanow, and K. Krajewski (1985), Jurrasic and Cretaceous lithostratigraphic units of the Tatra Mts, *Studia Geol. Pol.*, *84*, 1–86.
Lexa, J., et al. (2000), *Geological Map of Western Carpathians and Adjacent Areas 1: 500,000*, Minist. of the Environ. of Slovak Republic Geol. Surv. of Slovak Repub., Bratislava.
Maheľ, M. (1986), *Geological Structure of Czechoslovak Carpathians: Paleoalpine Units* [in Slovak], pp. 1–503, Veda, Bratislava.
Maluski, H., P. Rajlich, and P. Matte (1993), ^{39}Ar-^{40}Ar dating of the Inner Carpathians Variscan basement and Alpine mylonitic overprinting, *Tectonophysics*, *223*, 313–337.
Marschalko, R. (1968), Facies distribution, paleocurrents and paleotectonics of the Paleogene Flysch of Central West Carpathians, *Geol. Carpathica*, *19*, 69–94.
Marynowski, L., A. Gawęda, S. Cebulak, and M. Jędrysek (2001), Hydrocarbons migration in tectonic zones of the Western Tatra Mounyains crystalline basement (Central Western Carpathians), *Geol. Carpathica*, *52*, 3–14.
Marynowski, L., A. Gawęda, P. Poprawa, M. Żywiecki, B. Kępińska, and H. Merta (2006), Origin of organic matter from tectonic zones in the Western Tatra Mountains crystalline basement, Poland: An example of bitumen-source rock correlation, *Mar. Pet. Geol.*, *23*, 261–279.
McDougall, I., and T. M. Harrison (1988), *Geochronology and Thermochronology by the 40Ar/39Ar Method*, 212 pp., Oxford Univ. Press, New York.
Moussallam, Y., D. A. Schneider, M. Janák, M. Thöni, and D. K. Holm (2012), Heterogeneous extrusion and exhumation of deep-crustal Variscan assembly: Geochronology of the Western Tatra Mountains, northern Slovakia, *Lithos*, *144–145*, 88–108.
Nemčok, J., et al. (1993), *Explanations to Geological Map of the Tatra Mts. 1:50 000* [in Slovak], 135 pp., Geologický Ústav Dionýza Štúra, Bratislava.
Nemčok, J., et al. (1994), *Geological Map of the Tatra Mountains*, Min. of Environ. of Slovak Repub., Geologický Ústav Dionýza Štúra, Bratislava.
Nemčok, M. (1993), Transition from convergence to escape: Field evidence from the West Carpathians, *Tectonophysics*, *217*, 117–142.
Nemčok, M., and J. Nemčok (1994), Late Cretaceous deformation of the Pieniny Klippen Belt, West Carpathians, *Tectonophysics*, *239*, 81–109.
Nemčok, M., F. Marko, M. Kováč, and L. Fodor (1989), Neogene tectonics and paleostress changes in the Czechoslovakian part of the Vienna basin, *Jahrb. Geol. Bundesanst.*, *132*(2), 443–458.
Olszewska, B. W., and J. Wieczorek (1998), The Paleogene of the Podhale Basin (Polish Inner Carpathians—Micropaleonthological perspective, *Przegląd Geol.*, *46*, 721–728.
Petrík, I., P. Nabelek, M. Janák, and D. Plašienka (2003), Condition of formation and crystallization kinetics of highly oxidized pseudotachylytes from the High Tatras (Slovakia), *J. Petrol.*, *44*, 901–927.
Piotrowski, J. (1978), Mesostructural analysis of the main tectonic units of the Tatra Mts [In Polish with English summary], *Studia Geol. Pol.*, *55*, 1–80.
Plašienka, D. (2003), Development of basement-involved fold and thrust structures exemplified by the Tatric- Fatric-Veporic nappe system of the Western Carpathians (Slovakia), *Geod. Acta*, *16*, 21–38.
Plašienka, D., P. Grecula, M. Putiš, D. Hovorka, and M. Kováč (1997), Evolution and structure of the Western Carpathians: An overview, in *Geological Evolution of the Western Carpathians*, edited by P. Grecula, D. Hovorka, and M. Putiš, pp. 1–24, Miner. Slovaca Corp., Geocomplex, Bratislava, Slovak Republic.
Poller, U., and W. Todt (2000), U-Pb single zircon data of granitoids from the High Tatra Mountains (Slovakia): Implications for geodynamic evolution. Transactions of the Royal Society of Edinburgh, *Earth Sci.*, *91*, 235–243.
Poller, U., W. Todt, M. Janak, and M. Kohut (1999), The relationship between the Variscides and the Western Carpathians basement: New Sr, Nd and Pb-Pb isotope data from the Tatra Mountains, *Geol. Carpathica*, *50*, 131–133.
Poller, U., M. Janák, M. Kohút, and W. Todt (2000), Early Variscan magmatism in the Western Carpathians: U–Pb zircon data from granitoids and orthogneisses of the Tatra Mountains (Slovakia), *Int. J. Earth Sci.*, *89*, 336–349.
Poprawa, P., J. Grabowski, and I. Grotek (2002), Thermal and burial history of the sub-Tatric nappes and the Podhale basin—Constraints from preliminary maturity analysis and modelling, *Geologica Carpathica* 53 (special issue), Proceedings of the XVII CBGA, Bratislava.
Putiš, M. (1992), Variscan and Alpidic nappe structures of the Western Carpathian crystalline basement, *Geol. Carpathica*, *43*(6), 369–380.
Ratschbacher, L., O. Merle, P. Davy, and P. Cobbold (1991a), Lateral extrusion in the Eastern Alps. 1. Boundary conditions and experiments scaled for gravity, *Tectonics*, *10*, 245–256, doi:10.1029/90TC02622.

Ratschbacher, L., W. Frisch, H. G. Linzer, and O. Merle (1991b), Lateral extrusion in the eastern Alps, 2, Structural analysis, *Tectonics*, *10*, 257–271, doi:10.1029/90TC02623.
Ratschbacher, L., W. Frisch, H. G. Linzer, B. Sperner, M. Meschede, K. Decker, M. Nemčok, J. Nemčok, and R. Grygar (1993), The Pieniny Klippen Belt in the Western Carpathians of northeastern Slovakia: Structural evidence for transpression, *Tectonophysics*, *226*, 471–483.
Reiners, P. W. (2005), Zircon (U-Th)/He thermochronometry, in *Low-Temperature Thermochronology: Techniques, Interpretations, and Applications*, *Rev. Mineral. Geochem.*, vol. 58, edited by P. W. Reiners and T. A. Ehlers, pp. 151–176, Chantilly.
Reiners, P. W., T. L. Spell, S. Nicolescu, and K. A. Zanetti (2004), Zircon (U-Th)/He thermochronometry: He diffusion and comparisons with 40Ar/39Ar dating, *Geochim. Cosmochim. Acta*, *68*, 1857–87.
Rögl, F. (1996), Stratigraphic correlation of the Paratethys Oligocene and Miocene, *Mitt. Ges. Geol. Bergbaustud. Österr.*, *41*, 65–73.
Roniewicz, P. (1969), Sedymentacja eocenu numulitowego Tatr (Sedimentation of the Nummulite Eocene in the Tatra Mts), *Acta Geol. Pol.*, *19*, 503–608.
Royden, L. H., F. Horváth, and B. C. Burchfiel (1982), Transform faulting, extension, and subduction in the Carpathian Pannonian region, *Geol. Soc. Am. Bull.*, *93*, 717–725.
Royden, L. H., F. Horváth, A. Nagymarosy, and F. Stegena (1983), Evolution of the Pannonian Basin System. 2. Subsidence and thermal history, *Tectonics*, *2*, 91–137, doi:10.1029/TC002i001p00091.
Sachsenhofer, R. (2001), Syn- and post-collisional heat flow in the Cenozoic Eastern Alps, *Int. J. Earth Sci.*, *90*, 579–92.
Sachsenhofer, R. F., A. Lankreijer, S. Cloetingh, and F. Ebner (1997), Subsidence analysis and quantitative basin modelling in the Styrian Basin (Pannonian Basin system, Austria), *Tectonophysics*, *272*, 175–196.
Shuster, D. L., and K. A. Farley (2005), ^{4}He/^{3}He thermochronometry: Theory, practice, and potential complications, *Rev. Mineral. Geochem.*, *58*(1), 181–203.
Shuster, D. L., R. M. Flowers, and K. A. Farley (2006), The influence of natural radiation damage on helium diffusion kinetics in apatite, *Earth Planet. Sci. Lett.*, *249*, 148–161.
Śmigielski, M., P. Krzywiec, H. Sinclair, C. Persano, F. Stuart, P. Aleksandrowski, and K. Pisaniec (2010), Mechanisms of uplift and erosion in the Carpathian thrust wedge and foreland basin: Low temperature thermochronology of the Tatra Mountains, southern Poland, 279 pp., *12-th International Conference on Thermochronology*, Glasgow, 16–20 August.
Śmigielski, M., P. Krzywiec, K. Pisaniec, F. Stuart, C. Persano, H. Sinclair, N. Oszczypko, and K. Sobien (2011), Inversion of the Central Carpathian Basin constrained using low temperature thermochronology and its implications for Carpathian orogenesis, *Geophys. Res. Abs.*, 13, 12938.
Śmigielski, M., F. M. Stuart, P. Krzywiec, C. Persano, H. D. Sinclair, K. Pisaniec, and K. Sobien (2012), Dating the tectonic evolution of the Northern Carpathians (Poland) by zircon and apatite low temperature thermochronology, *13-th International Conference on Thermochronology*, 78 pp., Guilin, 24–28 August.
Sokołowski, S. (1959), Zdjęcia geologiczne strefy eocenu numulitowego wzdłuż północnego brzegu Tatr Polskich (sprawozdanie wstępne) (Geological map of the Nummulitic Eocene Region [northern marigin of the Polish Tatra]. Preliminary report), *Biuletyn Państwowego Inst. Geol.*, *149*, 197–213.
Soták, J. (2010), Paleoenvironmental changes across the Eocene-Oligocene boundary: Insights from the Central-Carpathian Paleogene Basin, *Geol. Carpathica*, *61*(5), 393–418.
Soták, J., M. Pereszlenyi, R. Marschalko, J. Milička, and G. Starek (2001), Sedimentology and hydrocarbon habitat of the submarine-fan deposits of the Central Carpathian Paleogene Basin (NE Slovakia), *Mar. Pet. Geol.*, *18*, 87–114.
Sperner, B. (1996), Computer programs for the kinematic analysis of brittle deformation structures and the Tertiary tectonic evolution of the Western Carpathians (Slovakia), Tübinger Geowiss. Arbeiten, Reihe A, Band 27, 120.
Sperner, B., L. Ratschbacher, and M. Nemčok (2002), Interplay between subduction retreat and lateral extrusion: Tectonics of the Western Carpathians, *Tectonics*, *21*(6), 1–24, doi:10.1029/2001TC901028.
Środoń, J., M. Kotarba, A. Biroń, P. Such, N. Clauer, and A. Wójtowicz (2006), Diagenetic history of the Podhale-Orava Basin and the underlying Tatra sedimentary structural units (Western Carpathians): Evidence from XRD and K-Ar of illite-smectite, *Clay Miner.*, *41*, 751–774.
Starek, D. (2001), Sedimentology and paleodynamics of the Paleogene formations of the Central Western Carpathians, pp. 1–152, Slovak Acad. Sci., Bratislava.
Starek, D., L. Sliva, and R. Vojtko (2012), Eustatic and tectonic control on late Eocene fan delta development (Orava Basin, Central Western Carpathians), *Geol. Q.*, *56*(1), 67–84.
Stegena, L., B. Geczy, and F. Horváth (1975), Late Cenozoic evolution of the Pannonian basin, *Tectonophysics*, *26*(1–2), 71–90.
Struzik, A., M. Zattin, and R. Anczkiewicz (2002), Timing of uplift and exhumation of the Polish Western Carpathians, *Geotemas*, *4*, 151–154.
Tari, G., F. Horváth, and J. Rumpler (1992), Styles of extension in the Pannonian Basin, *Tectonophysics*, *208*, 203–219.
Tari, G., P. Dövényi, I. Dunkl, F. Horváth, L. Lenkey, M. Stefanescu, P. Szafián, and T. Tóth (1999), Lithospheric structure of the Pannonian basin derived from seismic, gravity and geothermal data, in *The Mediterranean Basins: Tertiary Extension Within the Alpine Orogen*, edited by B. Durand et al., *Geol. Soc. London, Spec. Publ.*, *156*, 215–250.
Tokarski, A. K., A. Świerczewska, W. Zuchiewicz, D. Starek, and L. Fodor (2012), Quaternary exhumation of the Carpathians: A record from the Orava-Nowy Targ Intramontane Basin, Western Carpathians (Poland and Slovakia), *Geol. Carpathica*, *63*(4), 257–266.
Uhlig, V. (1899), Die Geologie des Tatragebirges, *Denkschr. Akad. Wiss. (Wien) Math.–Naturwiss. Kl.*, *68*, 1–87.
Vojtko, R., E. Tokárová, L. Sliva, and I. Pešková (2010), Reconstruction of Cenozoic paleostress fields and revised tectonic history in the northern part of the Central Western Carpathians (the Spišská Magura and Východné Tatry Mountains), *Geol. Carpathica*, *61*(3), 211–225.
Wagner, G., and P. Van den Haute (1992), *Fission-Track Dating*, 285 pp., Kluwer Acad., Dordrecht.
Wagner, M. (2011), Petrologic studies and diagenetic history of coaly matter in the Podhale flysh sediments, southern Poland, *Ann. Soc. Geol. Pol.*, *81*, 173–183.
Watycha, L. (1976), The Neogene of the Orava-Nowy Targ Basin [in Polish with English summary], *Kwart. Geol.*, *20*, 575–585.
Wolska, A., J. Szulc, and E. Koszowska (2002), K/Ar dating of the Middle Triassic tuffs from the Central Carpathians and its paleotectonic context, in *Proceedings ESSEWECA*, pp. 73–74, Institute of Geology, Slovak Academy of Science, Bratislava.
Wortel, M. J. R., and W. Spakman (2000), Subduction and slab detachment in the Mediterranean-Carpathian region, *Science*, *290*, 1910–1917.
Zaun, P., and G. A. Wagner (1985), Fission track stability in zircon under geological conditions, *Nucl. Tracks Radiat. Meas.*, *10*, 303–307.
Żytko, K., R. Zając, S. Gucik, W. Ryłko, N. Oszczypko, I. Garlicka, J. Nemčok, M. Eliáš, E. Menčík, and Z. Stráník (1989), Map of the tectonic elements of the Western Outer Carpathians and their foreland 1:500 000, in *Geological Atlas of the Western Outer Carpathians and Their Foreland*, edited by D. Poprawa and J. Nemčok, Państwowy Inst. Geol., Warszawa.